Chromospheric activity of periodic variable stars (including eclipsing binaries) observed in DR2 LAMOST stellar spectral survey

Liyun Zhang[*,a], Hongpeng Lu[a], Xianming L. Han[a,b], Linyan Jiang[a], Zhongmu Li[c], Yong Zhang[d], Yonghui Hou[d], Yuefei Wang[d], Zihuang Cao[e]

[a] *Department of Physics and Astronomy, College of Physics, Guizhou University, Guiyang 550025, PR China*
[b] *Department of Physics and Astronomy and SARA, Butler University, Indianapolis, IN 46208, USA*
[c] *Institute for Astronomy and History of Science and Technology, Dali University, Dali 671003, China*
[d] *Nanjing Institute of Astronomical Optics & Technology, National Astronomical Observatories, Chinese Academy of Sciences, Nanjing 210042, PR China*
[e] *Key Laboratory of Optical Astronomy, National Astronomical Observatories, Chinese Academy of Sciences, Beijing 100012, PR China*

ARTICLE INFO

ABSTRACT

The LAMOST spectral survey provides a rich databases for studying stellar spectroscopic properties and chromospheric activity. We cross-matched a total of 105,287 periodic variable stars from several photometric surveys and databases (CSS, LINEAR, Kepler, a recently updated eclipsing star catalogue, ASAS, NSVS, some part of SuperWASP survey, variable stars from the Tsinghua University-NAOC Transient Survey, and other objects from some new references) with four million stellar spectra published in the LAMOST data release 2 (DR2). We found 15,955 spectra for 11,469 stars (including 5398 eclipsing binaries). We calculated their equivalent widths (*EWs*) of their H_α, H_β, H_γ, H_δ and Ca ii H lines. Using the H_α line EW, we found 447 spectra with emission above continuum for a total of 316 stars (178 eclipsing binaries). We identified 86 active stars (including 44 eclipsing binaries) with repeated LAMOST spectra. A total of 68 stars (including 34 eclipsing binaries) show chromospheric activity variability. We also found LAMOST spectra of 12 cataclysmic variables, five of which show chromospheric activity variability. We also made photometric follow-up studies of three short period targets (DY CVn, HAT-192-0001481, and LAMOST J164933.24 + 141255.0) using the Xinglong 60-cm telescope and the SARA 90-cm and 1-m telescopes, and obtained new BVRI CCD light curves. We analyzed these light curves and obtained orbital and starspot parameters. We detected the first flare event with a huge brightness increase of more than about 1.5 magnitudes in R filter in LAMOST J164933.24 + 141255.0.

1. Introduction

Many periodic variables (especially those with late spectral type) exhibit magnetically active phenomena, such as starspots, chromospheric plages and flares, coronal emissions (Güdel, 2002; Berdyugina, 2005; Hall, 2008; Strassmeier, 2009). These phenomena are important for determining rotational and magnetic-related activity properties in the photosphere, chromosphere, transition region and corona at different stages of stellar evolution (Messina et al., 2001). Stellar magnetic activity produces fill-in or emission in several activity-sensitive spectral lines, especially the H_α (6563 Å), H_β (4861 Å), H_γ (4341 Å), H_δ (4102Å), H_8 (3889Å), and Ca ii H (3968Å) & K (3933Å), and Ca ii IRT lines (Sobolev et al., 1982; Montes et al., 2001; West et al., 2011; Zhang et al., 2015; 2017; etc). These lines serve as chromospheric activity indicators. The H_α emission is the most common and prominent spectroscopic feature of T Tau stars (Reipurth et al., 1996). The emission in

H_α line may arise from several different mechanisms: stellar magnetic activity of solar type, star-star interaction (especially in the RS CVn systems), star-disk interactions (especially in classical T Tauris stars), star-planet interaction, (Karoff et al., 2016; Frasca et al., 2016; Reipurth et al., 1996). Researchers have discovered that many M stars are active and studied the depdendence of their level of activity on spectral type using the SDSS and LAMOST surveys, and determined the space distribution of active stars within our Milky Way (West et al., 2011; Yi et al., 2014; Zhang et al., 2016; Fang et al., 2016). Frasca et al. (2016) studied LAMOST spectra as part of the spectroscopic follow-up observations of Kepler survey by using the spectral subtraction of inactive templates using the code ROTFIT and derived the fluxes of several lines sensitive to magnetic activity. The rotation periods determined from the Kepler photometry allowed to study the dependence of the chromospheric fluxes and the amplitude of light curve variations on the rotation rates. Similarly, our main motivation is to build a large catalog of

---

Table 1
List of photometric surveys and corresponding number of stars and LAMOST spectra analysed in this study.

Survey source	Number of variable star			Number of eclipsing binary			Reference
Survey source	Total	Spectra	object	Total	Spectra	Object	Reference
CSS	47,000	6608	4862	35,581	5255	3826	Drake et al. (2014a)
LINEAR	7000	1654	1209	2742	576	437	Sesar et al. (2011); Palaversa et al. (2013)
Kepler	34,030	6155	4891	2878	868	676	Prša et al. (2011); Abdul-Masih et al. (2016); McQuillan et al. (2014)
eclipsing catalogue	7200	1631	849	7200	1631	849	Avvakumova et al. (2013)
ASAS	50,099	257	214	11,076	110	89	Pojmanske (2000; 2002; 2003)
Xinglong 80-cm Survey	1237	28	24	431	4	4	Yao et al. (2015)
NSVS	8678	593	462	2883	441	329	Wozniak (2004)
SuperWASP	143	18	14	143	18	14	Pollacco et al. (2006); Norton et al. (2007); Lohr et al. (2013)
other	11	11	11	11	11	11	Pribulla et al. (2012); Eker et al. (2008)
total	105,287	15,955	12,536	60,945	8914	6235	

stars with known rotation period and, possibly, also other stellar parameters and to measure their magnetic activity using LAMOST spectra. To accomplish our aim we have explored a number of catalogs and surveys that we will describe in the following:

Avvakumova et al. (2013) published a new and largest catalogue of eclipsing binaries. This catalogue contains parameters for 7200 stars. It also contains morphological type of the light curve, orbital period and information on period variability. Avvakumova et al. (2013) also analyzed stellar parameter distribution of eclipsing systems.

Drake et al. (2014a) used three telescopes covering the sky declination δ region ranging from −75 to +65 degrees and right ascension ranging from 0 to 360 degrees and discovered 47,000 periodic variables (including 31,000 eclipsing binaries) with the V magnitude ranging from 12 to 20 in the Catalina SKY Surveys (CSS) from 2004 (Drake et al., 2013a; 2013b). Drake et al. (2014b) also investigated the properties of 367 ultra-short period binary candidates from their 31,000 eclipsing binaries sources. They spectroscopically confirmed the existence of several M dwarf + M dwarf contact binaries.

Palaversa et al. (2013) visually confirmed and classified 7000 periodic variable stars in the 14–17 range of magnitudes from the asteroid survey of northern sky (LINEAR). The periodic LINEAR variables contain 3900 RR Lyrae stars, 2700 eclipsing binaries, and some other type of variable stars (Sesar et al., 2011).

The SuperWASP project (Pollacco et al., 2006) aimed at searching for transiting extrasolar planets using wide field photometric survey, which started in 2004. We obtain the coordinates of several hundred SuperWASP periodic variable stars (Norton et al., 2007; Lohr et al., 2013).

All Sky Automated Survey (ASAS) discovered 50,099 variable stars (including 11,076 eclipsing binaries) brighter than V = 14 mag south of declination +28 (Pojmanski, 1997; Pojmanski et al., 2005).

Northern Sky Variability Survey (NSVS) discovered 8678 slowly-rotating variable stars (including 2883 eclipsing binaries) covering the entire sky above declination +38° with magnitudes ranging from 8 to 15.5 mag in the V band (Wozniak et al. 2004).

The primary Kepler Mission provided nearly continuous monitoring of 200000 objects with unprecedented photometric precision. McQuillan et al. (2014) detected 34,030 stars with rotation periods between 0.2 and 70 days from 133,030 main-sequence Kepler targets. The final catalog of 2878 eclipsing binary systems in the Kepler field of view was presented by Abdul-Masih et al. (2016); Prša et al. (2011).

Yao et al. (2015) detected 1237 variable stars (including 661 RR Lyrae stars, 431 eclipsing binaries, and 299 new variables) with a brightness greater than 18.0 mag with periods ranging from a few hours

to a few hundred days from the first two years of observations from the Tsinghua University-NAOC Transient Survey at Xinglong station, NAOC. We also retrieved additional new variable stars, such as low-mass eclipsing binaries from Pribulla et al. (2012), and from the catalogue of chromospherically active binary stars (Eker et al., 2008; Strassmeier et al., 1993). Our goal is to make our catalogue as complete as possible. However, we do miss many other known periodic variables, especially bright stars that exceed the upper brightness limit in the LAMOST survey, and stars in unpublished catalogs.

A large number of stellar spectra were obtained from the spectroscopic survey of the Large Sky Area Multi-object Fiber Spectroscopic Telescope (LAMOST, aka Guo Shou Jing telescope) (Zhao et al., 2012; Luo et al., 2015), which allow to study chromospheric activity of periodic variable stars, and its dependence on stellar parameters. These large stellar spectroscopic survey and photometric survey will trigger detailed statistical studies of stellar physics and stellar magnetic activities. One disadvantage with NSVS, ASAS, LINEAR, CCT datasets is the lack of precision multi-color photometry, which can in principle provide more precise information on orbital inclinations, relative radius, and other orbital parameters in binary systems.

For many periodic stars that we retrieved from photometric surveys, spectral type and magnetic activity are not known. Stellar spectra from LAMOST survey fill this important information gap nicely. In our paper, we cross-matched the LAMOST catalog with the above mentioned photometric catalogs of periodic variable stars. Among the periodic variable stars that have one or more LAMOST spectra, we search for chromospheric active stars. Then, we measured the EW of a selection of lines that are sensitive to magnetic activity. However, because our method, we could identify only very active stars, that is stars whose very high level of magnetic activity has filled in their lines and thus are observed in emission. Therefore, we do not search for any correlation with spectral type, binary, orbital period. Conversely, there are also stars with available spectra from LAMOST survey but without detailed multi-bands photometric information. For this reason, we selected several interesting targets with strong chromospheric activities, and further investigate their properties using photometric follow-up observation. Although the variables and eclipsing variables with longer periods can have prominent activity, we only focus on short-period eclipsing variables because of limited telescope time for the photometric follow-up. To better understand the photospheric starspot activities and orbital parameters of short period eclipsing binaries, we monitored some of them with multi-color CCD photometry using several optical telescopes. We obtained light curves of three eclipsing binaries: DY CYn, HAT-192-0001481 (2MASS J16121668 + 4113509)

Table 2
Parameters of LAMOST spectra for the targets analysed in this study.

LAMOST name	date	SN u	g	r	i	z	Sp.T	Magnitudes Filters	Mag1	Mag2	Mag3	Mag4	Mag5	Mag6	Mag7	Teff K	logg cm s^{-2}	Survey	Period d	LC Amplitude mag	Survey No
J011355.38+303033.1	2012-1-5	0	5.89	8.05	7.36	7.65	G0	ugrizjh	99	16.74	16.19	16.03	99	99	99			CSSECLi	6.3967600	0.18	J011355.3+303033
J011404.05+390557.9	2011-12-28	1.45	8.34	11.99	12.73	6.62	F5	ugrizjh	99	15.38	15.06	14.95	99	99	99	6020.26	4.112	CSSECLi	0.402634	0.19	J011404.0+390557
J011409.68+394305.8	2011-12-28	1.25	6.45	12.38	16.85	10.68	K2	ugrizjh	99	15.65	14.82	14.55	99	99	99	4903.17	3.891	CSSECLi	0.289368	0.17	J011409.7+394306
J011413.32+354953.2	2013-9-26	4.01	22.07	33.06	31.52	19.27	A7V	ugrizjh	99	15.08	14.77	14.86	99	99	99			CSSECLi	0.447016	0.11	J011413.3+354953
J011418.24+373651.0	2012-10-7	1.37	3.69	5.99	8.63	6.01	F5	ugrizjh	99	15.26	14.92	14.97	99	99	99			CSSECLi	0.348866	0.21	J011418.2+373651
J011434.89+432057.3	2013-11-23	2.04	33.39	60.44	87.19	61.97	K5	ugrizjh	18.01	15.89	14.2	14.24	14.09	99	99	4560.54	4.4	CSSECLi	0.253229	0.26	J011434.8+432057
J011459.64+421054.4	2013-10-24	9.99	34.47	64.6	77.82	56.4	G7	gri	14.73	14.25	14.2	99	99	99	99	5209.33	3.787	CSSECLi	0.250156	0.37	J011459.7+421052
J011530.73+384244.3	2013-11-25	1.99	10.7	15.61	16.4	7.28	A6IV	ugrizjh	99	17.84	17.58	17.67	99	99	99			CSSECLi	0.35782	0.38	J011530.7+384244
J011553.72+375504.1	2012-10-7	1.56	3.75	7.36	10.18	6.72	G7	ugrizjh	99	16.06	15.88	15.51	99	99	99			CSSECLi	0.33589	0.30	J011553.7+375504
J011611.79−065936.7	2012-9-30	12.21	23.31	6.21	5.18	5.89	G3	gribvjh	13.21	12.58	12.15	13.59	12.79	11.24	10.92	5777.77	4.385	CSSECLi	0.387904	0.34	J011611.8−065936
J011616.83+224722.4	2012-10-30	1.56	1.88	3.9	4.57	4.33	Non	gribvjh	14.13	13.31	12.98	14.65	13.68	11.64	11.14			CSSECLi	0.258554	0.52	J011616.8+224722
J011628.86+401044.2	2013-12-13	11.5	36.5	51.34	47.05	30.56	G3	brijhk	15.11	13.97	13.48	12.23	12.39	12.06	12	5584.85	4.052	CSSECLi	0.383396	0.43	J011628.8+401044
J011638.70+442439.0	2013-11-23	3.17	18.48	24.35	22.65	13.2	A6IV	ugrizjh	99	14.8	14.75	14.55	99	99	99			CSSECLi	0.525768	0.32	J011638.8+442438
J011714.49+245824.7	2012-10-1	7.17	15.13	9.5	14.63	14.03	F9	gribvjh	14.49	13.63	13.3	14.97	13.98	12.14	11.55	5138.62	3.866	CSSECLi	0.256288	0.47	J011714.5+245824
J011727.63+322105.0	2011-12-13	5.61	33.62	46.19	80.82	67.24	G4	ugrizjh	99	14.28	13.68	13.44	99	99	99	5634.15	4.068	CSSECLi	0.457348	0.12	J011727.6+322105
J011738.07+031958.9	2012-10-31	1.83	3.73	3.11	2.51	2	G0	ugriz	16.67	15.57	15.21	15.08	15.04	99	99			CSSECLi	0.55671	0.17	J011738.0+031959
J011744.81+283118.1	2012-12-5	1.53	7.34	9.14	12.87	7.09	G4	griz	16.49	15.97	15.78	15.68	99	99	99			CSSECLi	0.340686	0.35	J011744.8+283118
J011804.13+315032.3	2013-10-4	3.23	22.26	36.01	51.08	34.29	G3	brijhk	15.99	13.79	14.16	13.52	13.3	12.9	12.87	5581.96	4.066	CSSECLi	1.17684	0.09	J011804.1+315032
J011818.53−005643.6	2013-11-7	1.34	6.72	11.02	19.22	12.93	K7	ugrizri	19.37	17	15.8	15.29	14.98	16.06	15.55	3929.17	4.261	CSSECLi	0.5544320	0.45	J011818.5−005643
J011822.48+080543.7	2013-9-23	5.84	15.3	16.12	10.77	9	F5	ugriz	16.16	15.03	14.65	14.51	14.46	99	99	5842.39	3.853	CSSECLi	0.454696	0.20	J011822.4+080543
J011832.83−055854.0	2012-9-30	21.92	47.78	8.88	5.45	4.79	F9	gribvjh	15.72	14.88	14.48	16.31	15.26	13.13	12.57	5226.61	3.829	CSSECLi	0.382141	0.55	J011832.7−055854
J011915.02+313527.0	2013-10-4	7.64	41.16	63.39	83.63	57.09	F7	brijhk	14.55	12.53	12.83	12.3	12.1	11.84	11.77	5920.38	4.098	CSSECLi	0.434313	0.31	J011915.0+313527
J011941.09+311205.0	2013-10-4	31.42	115.56	192.08	244.21	183.43	F7	brijhk	11.84	11.05	99	12.01	10.22	9.96	9.89	6189.66	4.164	CSSECLi	0.55399	0.55	J011941.1+311205
J012025.48+001624.9	2012-10-31	1.46	7.07	13.78	9.33	8.61	G2	gribvjh	14.06	13.52	13.23	14.4	13.7	12.35	12.04			CSSECLi	0.372246	0.49	J012025.4+001625
J012044.50+331732.3	2013-12-23	5.16	18.05	24.43	26.06	12.25	A3IV	ugrizjh	99	17.38	17.27	17.28	99	99	99			CSSECLi	0.36136	0.36	J012044.5+331732
J012052.97+263141.7	2012-12-5	6.31	53.74	74.11	88.65	62.88	F0	gribvjh	14.65	14.26	14.15	14.98	14.41	13.26	13	6727.68	4.225	CSSECLi	0.4225817	0.26	J012052.9+263141
...	...						...	...	...	...	...	...	...	...	...			...	...	...	...

This table is available in its entirety in machine-readable and Virtual Observatory (VO) forms in the online journal. A portion is shown here for guidance regarding its form and content.
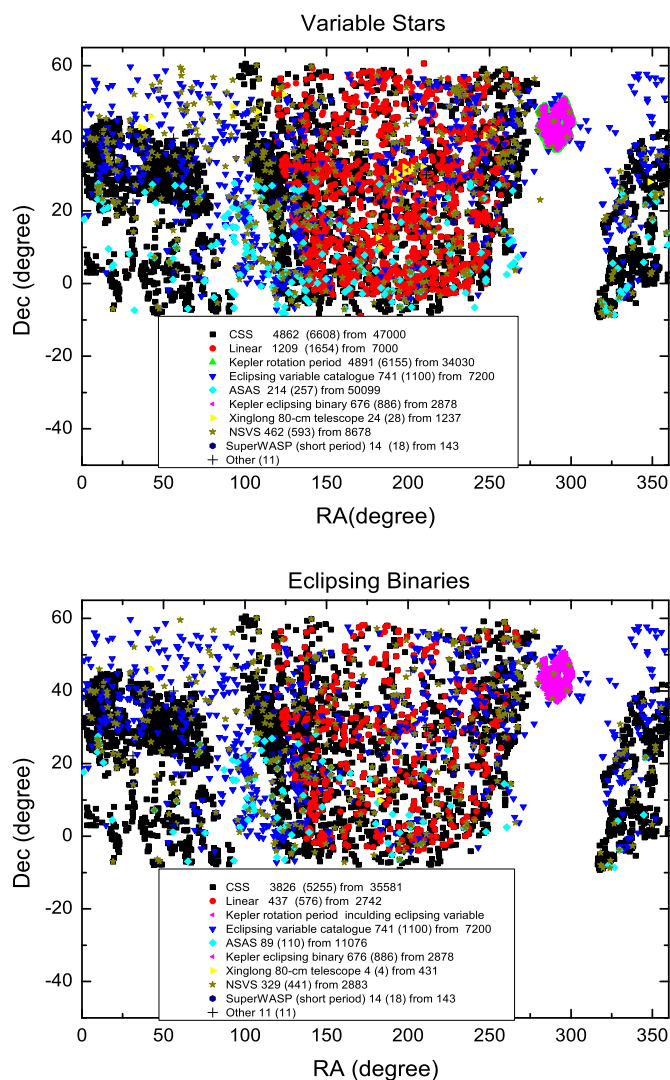
Fig. 1. Spatial distributions of periodic variable stars and eclipsing binaries discovered by different surveys. Different symbols and colors represent different stellar surveys.
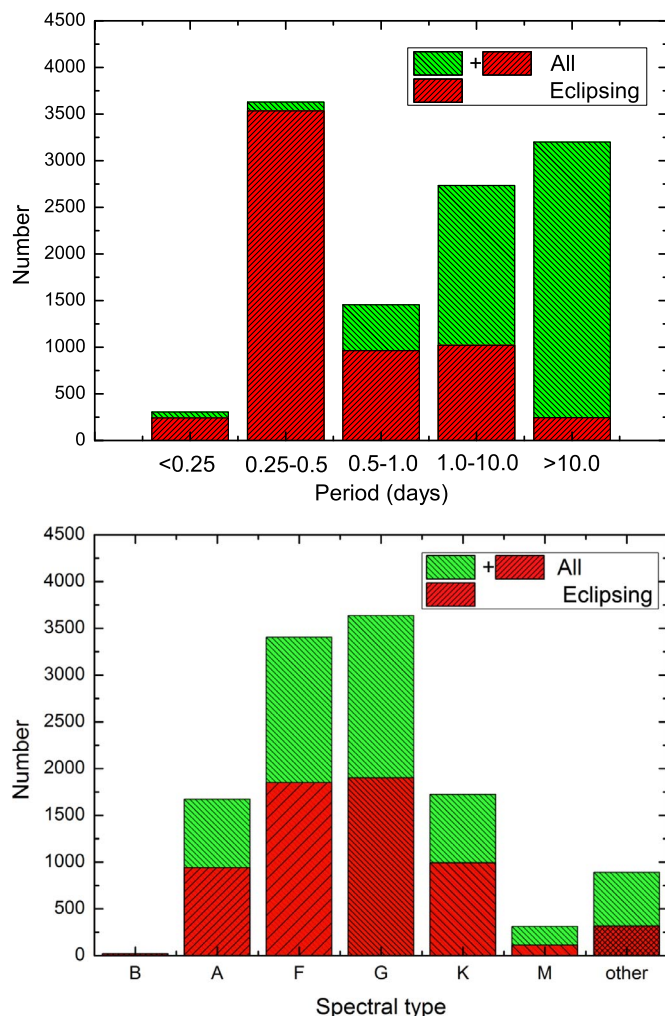

Fig. 2. Population distribution in terms of orbital periods and spectra types for all stars and eclipsing binaries considered in this study and present in the LAMOST Survey.

and LAMOST J164933.24 + 141255.0. By analyzing these light curves, we obtained their physical and starspot parameters.

2. LAMOST spectral survey

LAMOST is a telescope with aperture of about 4 m and a field of view of 5 square degrees and located at Xinglong station, National Astronomical Observatories of China (NAOC). The telescope can simultaneously obtain the spectra of about 4000 stars with low-resolution of about 1800 in a single exposure (Wang et al., 1996; Cui et al., 2012). Its spectroscopic survey released over four million spectra in December, 2015 (Zhao et al., 2012; Liu et al., 2015; Luo et al., 2012; 2015). It also obtained low-resolution spectra for objects in the Kepler field of view (De Cat et al., 2015)). The huge amount of DR2 spectra obtained by LAMOST survey can be used to study stellar astrophysics and structure of Galaxy and are important for analyzing the spectral properties of variable stars (including eclipsing binaries).

We cross matched 105,287 periodic variable stars from the

mentioned photometric surveys (CSS, LINEAR, Kepler, eclipsing binary catalogue, ASAS, NSVS, some part of SuperWASP survey, the Tsinghua University-NAOC Transient Survey, and other objects from some newly references.) with four million LAMOST stellar spectra (LAMOST data release 2, DR2). We selected spectra with signal to noise values greater than 5. We found 15,955 such spectra (8914 of them for eclipsing binaries) for a total of 12,536 variable stars (including 6235 eclipsing binaries). The results of our cross-match are summarized in Table 1. In the online version of this paper, we also present four electronic catalogues (cat1, cat2, cat3, and cat4) for all the variable stars. Cat1 lists the spectral parameters of the variable stars and Cat2 lists the stars' parameters. Cat3 lists the spectral parameters of eclipsing binaries and Cat4 lists the stellar parameters of eclipsing binaries. These electronic Tables include star names, right ascensions (RA) and declinations (DEC), observation dates, spectral types, magnitudes, signal to noise ratios (SN), and the photometric survey, the orbital periods, and the types of variable stars (eclipsing binary, RR Lyr variable star, and others). We listed part of the parameters of some targets in Table 2. The individual LAMOST spectra can be downloaded from the LAMOST web site (http://dr2.lamost.org/). We plotted the spatial distribution of all the periodic

Table 3

Spectral parameters of chrompsheric activity indicators of LAMOST targets.

| LAMOST name	Date	HJD-2400000	EXpo	Sp.T	H_α		H_β		H_γ		H_δ		CaH		Survey
	Day	d	Second		EWÅ	diff	EWÅ	diff	EWÅ	diff	EWÅ	diff	EWÅ	diff	
J190036.96+415600.2	2014-06-02T18:57:40.56	56811.13681	1800	G8	-1.01317	23.2329559	-1.4433925	6.9032512	-0.7908074	1.5181185	-1.1310529	2.7548544	-4.1274977	1.2353747	Kep
J185953.14+415018.2	2014-06-02T18:57:40.56	56811.13681	1800	F9	-1.49298	6.9620876	-2.0197163	11.1408033	-1.9123414	2.3445168	-1.8789489	4.5196590	-4.5398188	1.5295621	Kep
J185924.64+415912.3	2014-06-02T18:57:40.56	56811.13681	1800	Non	-0.0765888	2.9206781	-0.8269560	2.1853607	-2.2797778	2.7803953	-1.6691663	4.6031246	5.3650494	2.5562110	Kep
J185851.49+412711.7	2014-06-02T18:57:40.56	56811.13681	1800	F0	-1.74412	6.9805856	-2.5631139	8.4008894	-2.8027599	3.8947926	-2.6027474	5.9733906	-4.0598011	1.7356753	Kep
J185922.75+412841.7	2014-06-02T18:57:40.56	56811.13681	1800	G2	-1.29725	11.9368420	-1.8288707	11.3726530	-1.4161639	1.9608554	-1.6605034	4.8414516	-4.5923872	2.0618172	Kep
J185902.20+411150.7	2014-06-02T18:57:40.56	56811.13681	1800	F0	-1.59638	5.4541745	-2.4318323	10.8862095	-2.5531499	4.0716085	-2.5315733	6.8919253	-3.4893525	1.7023852	Kep
J185843.96+412607.8	2014-06-02T18:57:40.56	56811.13681	1800	G8	-0.978203	25.6771145	-1.3770964	7.8395195	-0.6476979	1.3735858	-1.0090338	2.0004354	-3.8865590	1.0578030	Kep
J185752.37+412730.7	2014-06-02T18:57:40.56	56811.13681	1800	G7	-1.03673	11.8867798	-1.2643517	8.0916643	-0.4690576	1.1516701	-1.0036939	2.0147786	-4.8266368	2.8655746	Kep
J185650.83+413012.6	2014-06-02T18:57:40.56	56811.13681	1800	G7	-1.07840	13.5702105	-1.3547561	10.1004095	-0.7054844	1.5170816	-0.9576936	2.5780382	-4.7500644	1.8380400	Kep
J185627.28+413556.7	2014-06-02T18:57:40.56	56811.13681	1800	F6	-1.57214	6.6546865	-2.2888443	13.0482302	-2.3871365	3.5026963	-2.1851487	7.1475978	-4.3337073	2.2405987	Kep
J185454.55+413915.7	2014-06-02T18:57:40.56	56811.13681	1800	G3	-1.09233	4.6063437	-1.6311367	4.5818715	-0.9187644	1.6569855	-1.0061871	4.9249167	-4.0266709	3.1761808	Kep
J185854.35+421229.5	2014-06-02T18:57:40.56	56811.13681	1800	G3	-1.16984	3.4690461	-1.4974930	6.2669573	-1.2440525	2.2659178	-1.5850347	2.7053969	-2.4986639	2.914186	Kep
J220955.96-003850.3	2011-10-24T12:07:14.18	55858.87153	5400	A6V	-0.171611	1.4576762	-1.8314699	9.0944456	-2.0410216	6.4239316	-2.8160930	5.8889284	-1.3426030	2.9073238	CSS
J220345.09-003216.4	2011-10-24T12:10:52.15	55858.87153	5400	A2V	1.08771	1.0761257	-1.0740727	2.4828985	-2.1044273	2.1167269	-1.2536711	4.9336371	0.8006388	1.5795645	CSS
J220234.00+011421.2	2011-10-24T12:08:03.00	55858.87153	5400	A7V	-0.993358	1.6883099	-2.4508200	6.8364749	-2.8223581	2.8051147	-2.9400799	2.8679183	-1.2418541	1.3168759	CSS
J220128.62+004712.5	2011-10-24T12:08:03.00	55858.87153	5400	A6IV	-1.29501	1.5354640	-2.0786850	4.5060353	-1.9988842	2.2339530	-1.7897393	4.4842148	-1.1319811	2.1157994	CSS
J030037.57-023229.0	2011-10-24T16:26:29.88	55859.05000	5400	Non	-3.36539	1.5538270	-3.1910090	3.1910889	-1.9184986	1.6587127	-3.8816075	4.3416996	-7.7390590	4.8225102	CSS
J030652.91-020332.6	2011-10-24T16:26:39.92	55859.05000	5400	G0	-1.48906	1.4043077	-0.4894491	2.8466680	0.0489922	3.3256903	-3.1347611	4.1305099	-2.4837122	6.2111368	CSS
J030504.12+000450.0	2011-10-24T16:27:16.91	55859.05000	5400	G7	-0.541453	1.8206453	-1.0491741	3.5338597	-0.6876576	1.3326645	-0.9453005	2.1769538	-3.2189777	0.5522291	CSS
J004219.81+400838.5	2011-10-24T14:12:37.57	55858.94514	3600	G7	0.289357	1.8339646	-1.2646148	2.6437278	-1.9013541	2.0630205	-0.9672137	3.6701863	-2.6211748	8.5917845	CSS
J220644.68+291028.1	2011-10-25T12:23:43.79	55859.87083	3600	Non	0.428263	2.5918536	-1.4745468	2.6114357	-1.1619440	4.1697140	0.7492788	4.1728077	50.3069916	3.9600949	CSS
J222029.36+294550.3	2011-10-25T12:20:31.92	55859.87083	3600	G2	-0.546403	1.8975923	-1.2759409	10.4248619	-1.0220155	1.7980384	-1.4100147	3.8571911	-3.3872604	3.1907246	CSS
J221652.02+301402.2	2011-10-25T12:20:39.79	55859.87083	3600	K1	-0.287953	1.6278864	-1.3212373	1.8674942	0.7451056	1.9343764	0.8028975	4.2262988	-0.4465053	10.3201733	CSS
J221838.08+320807.2	2011-10-25T12:25:51.08	55859.87083	3600	K5	0.599840	1.3586771	-1.4102353	2.8866615	-0.3172737	2.5787444	-1.5723869	3.8617470	-3.7561395	3.4135623	CSS
J232745.55+292711.0	2011-10-27T12:42:08.23	55861.88333	3600	Non	0.733242	2.0172210	-0.6416138	2.3562460	-0.0293304	2.7631390	-0.1611187	2.3346708	-4.2229679	2.9219351	CSS
J233538.38+301527.4	2011-10-27T12:42:08.23	55861.88333	3600	K4	0.254136	1.0335567	-0.0286391	1.3589493	0.3259281	1.0439643	-0.4261265	1.3742567	-1.9946281	1.8968164	CSS
J234100.82+330959.4	2011-10-27T12:47:12.21	55861.88333	3600	G2	-0.609145	1.9842157	-1.7927811	2.8414478	-1.1629080	1.7962219	-2.0848310	3.7330341	-3.7012992	3.6938682	CSS
J234148.96+312417.4	2011-10-27T12:42:35.70	55861.88333	3600	M0	1.14580	3.2297325	-0.0217049	3.8928964	-1.0516282	1.8874346	1.3091003	1.9609549	-3.3293221	2.1981354	CSS
J234039.68+320905.7	2011-10-27T12:42:35.70	55861.88333	3600	K4	-0.0857605	1.0724305	-0.6774870	5.4907763	0.0905975	1.0515984	-0.4671314	3.5347130	1.0588760	3.4167776	CSS
J232406.03+324057.8	2011-10-27T12:41:53.93	55861.88333	3600	K5	0.364628	2.3803735	-1.5112716	4.4227200	1.2801425	3.9553120	0.5481787	2.9994864	-22.7238369	3.4319685	CSS
J232539.70+325954.2	2011-10-27T12:41:53.93	55861.88333	3600	K3	-0.0346129	2.1195900	-0.5678842	2.8698969	0.0207323	1.7316715	-0.5410025	2.2288368	-2.0278063	0.9078611	CSS
J035657.44+274931.9	2011-10-27T18:29:07.08	55862.08403	1200	F3	-1.32160	2.9997950	-2.5731685	4.2000194	-2.6575880	2.5932391	-2.4468853	3.8114724	-3.3269031	1.7453660	CSS

This table is available in its entirety in machine-readable and Virtual Observatory (VO) forms in the online journal. A portion is shown here for guidance regarding its form and content. "Diff" means the ratio between the height of the chromospheric activity line and its noise at the line center.

Table 4
Spectral parameters of active LAMOST targets.

| LAMOST name	Known?	Source name	Emission	Period d	Source Source	Date	HJD d	SN	Sp.T	EW(H$_\alpha$) Å	EW(H$_\beta$) Å
LAMOST J000205.28+381322.6	Unknown	SuperWASP	em	0.20908	sup	2012-11-30	56,261	11.52	K7	0.478 ± 0.055	-
LAMOST J000435.93+174001.0	Unknown	000436+1740.0	em	172.000000	ASAS	2012-9-28	56,198	79.99	K4	0.503 ± 0.006	-
LAMOST J000507.49+482705.0	Unknown	AM And	core	8.85051000	ecli	2013-10-30		177.330	A3IV	-	-15.214 ± 1.946
LAMOST J000507.49+482705.0	Unknown	AM And	core	8.85051000	ecli	2013-11-22		66.1600	A3IV	-	-14.317 ± 2.293
LAMOST J001242.47+252831.3	Unknown	CSS J001242.4+252831	em	106.04708	CSS	2013-10-10	56,575	60.51	M2	1.881 ± 0.028	2.538 ± 0.066
LAMOST J002142.41+381237.2	Unknown	CSS J002142.3+381237	em	2.58688	CSS	2012-10-31	56,231	11.15	K5	2.406 ± 0.176	-
LAMOST J002154.99+352348.1	Unknown	CSS J002154.9+352348	em	0.266826	CSS	2012-10-31	56,231	10.72	M0	1.873 ± 0.235	-
LAMOST J002607.18+250000.0	Unknown	CSS J002607.2+253802	em	0.555319	CSS	2012-11-24	56,255	28.12	K7	2.008 ± 0.002	-
LAMOST J002641.19+415921.7	Unknown	CSS J002641.1+415921	em	0.7110880	CSS	2012-12-4	56,265	43.13	K5	1.506 ± 0.032	-
LAMOST J003005.80+261726.3	Known	PX And	em	0.1463530064	ecli	2012-11-24			CV	47.738 ± 0.868	22.343 ± 0.187
LAMOST J005740.09+292956.5	Unknown	CSS J005740.1+292956	em	0.346171	CSS	2011-11-24	55,889	3.84	M3	5.837 ± 0.306	6.205 ± 0.137
LAMOST J005945.95+305335.0	Unknown	CSS J005945.9+305334	em	0.947248	CSS	2011-11-24	55,889	26.43	K7	1.396 ± 0.091	-
LAMOST J010222.93+375506.9	Unknown	CSS J010222.9+375506	em	236.183	CSS	2011-12-12	55,907	38.9	M6	-	-
LAMOST J010222.94+375506.9	Unknown	CSS J010222.9+375506	em	236.183	CSS	2012-11-23	56,254	99.41	M6	-	-
LAMOST J011638.70+442439.0	Unknown	CSS J011638.8+442438	em	0.525768	CSS	2013-10-21	56,586	17.52	A7IV	3.854 ± 0.066	4.757 ± 0.110
LAMOST J012119.09-001950.0	Unknown	CSS J012119.1-001950	em	0.207282	CSS	2013-10-29	56,594	31.89	K7	1.522 ± 0.039	-
LAMOST J012438.69-021620.7	Known	CSS J012438.6-021620	em	1.2043	CSS	2012-10-12	56,212	4.37	M2	6.517 ± 0.097	-
LAMOST J012656.70+332103.0	Unknown	CSS J012656.7+332103	em	0.9620286	CSS	2013-9-25	56,560	24.1	K7	1.464 ± 0.055	-
LAMOST J012902.50-033744.4	Unknown	CSS J012902.4-033744	em	0.32953	CSS	2014-1-9	56,666	20.16	M0	2.056 ± 0.036	-
LAMOST J012902.50-033744.4	Unknown	CSS J012902.4-033744	em	0.32953	CSS	2012-11-1	56,232	17.85	M0	2.345 ± 0.100	1.057 ± 0.013
LAMOST J012902.50-033744.4	Unknown	CSS J012902.4-033744	em	0.32953	CSS	2013-12-3	56,629	83.04	K7	1.771 ± 0.021	1.067 ± 0.020
LAMOST J012902.50-033744.4	Unknown	CSS J012902.4-033744	em	0.32953	CSS	2014-1-3	56,660	59.2	M0	1.647 ± 0.022	-
LAMOST J012902.50-033744.4	Unknown	CSS J012902.4-033744	em	0.32953	CSS	2013-10-29	56,594	39.38	M0	1.119 ± 0.045	-
LAMOST J013159.85+294922.0	Unknown	TT Tri	em	0.1396369934	ecli	2011-12-13			CV	22.536 ± 0.744	-
LAMOST J013159.85+294922.0	Unknown	TT Tri	em	0.1396369934	ecli	2011-11-21			CV	-	-
LAMOST J013622.94+210017.9	Unknown	CSS J013622.9+210017	em	0.459956	CSS	2013-10-23	56,588	49.78	M0	2.215 ± 0.111	2.232 ± 0.037
LAMOST J014056.63+343504.4	Unknown	CSS J014056.6+343504	em	1.6828078	CSS	2013-9-25	56,560	27.39	K5	0.927 ± 0.030	-
LAMOST J014215.48+285850.5	Unknown	CSS J014215.5+285850	em	5.17564	CSS	2012-1-13	55,939	21.55	M3	5.379 ± 0.345	4.544 ± 0.076
LAMOST J014215.48+285850.5	Unknown	CSS J014215.5+285850	em	5.17564	CSS	2011-12-11	55,906	40.93	M3	1.836 ± 0.032	-
LAMOST J014215.48+285850.5	Unknown	CSS J014215.5+285850	em	5.17564	CSS	2012-1-4	55,930	6.17	M3	4.009 ± 0.021	-
LAMOST J014414.83+285506.6	Unknown	CSS J014414.8+285506	em	0.410082	CSS	2011-12-11	55,906	12.75	M1	2.597 ± 0.022	2.923 ± 0.123
LAMOST J020202.37+193333.0	Unknown	CSS J020202.3+193332	em	6.09039	CSS	2012-10-3	56,203	24.6	M0	2.701 ± 0.029	1.990 ± 0.104
LAMOST J020202.37+193333.0	Unknown	CSS J020202.3+193332	em	6.09039	CSS	2012-10-3	56,203	7.43	M0	0.709 ± 0.031	-
...	...	...	...	...	...	...	...	...	...	...	...

This table is available in its entirety in machine-readable and Virtual Observatory (VO) forms in the online journal. A portion is shown here for guidance regarding its form and content.
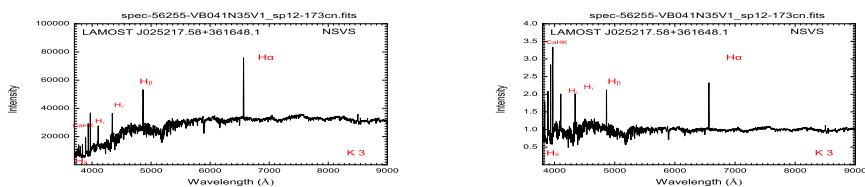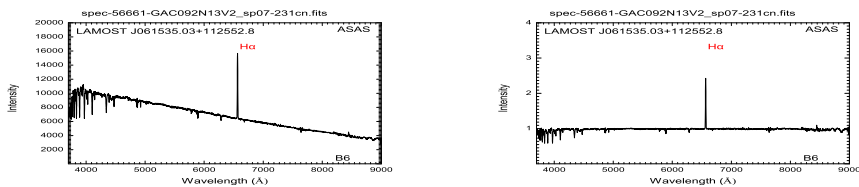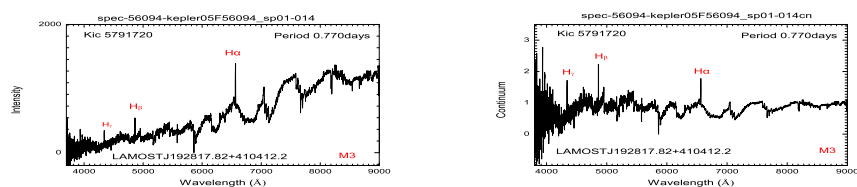
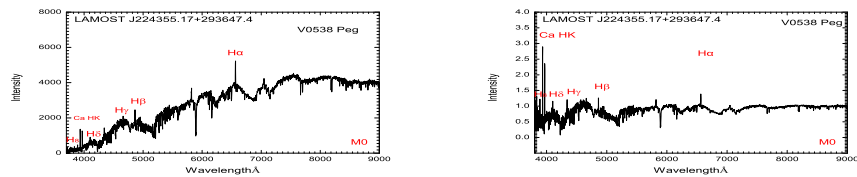(a) LAMOST J025217.58+361648.1
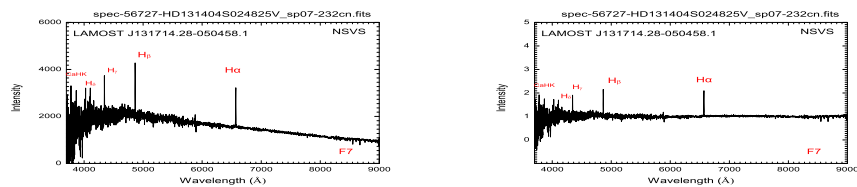
(b) LAMOST J131714.28-050458.1cn
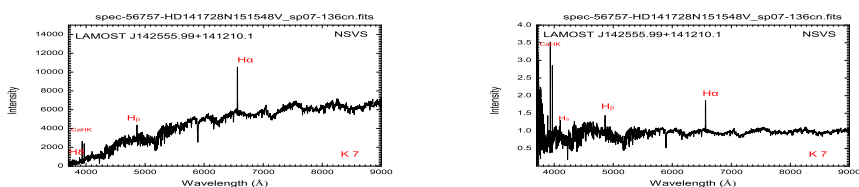
(c) LAMOST J142555.99+141210.1cn
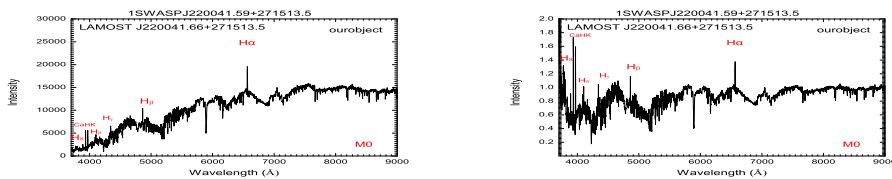
(d) LAMOST J061535.03+112552.8
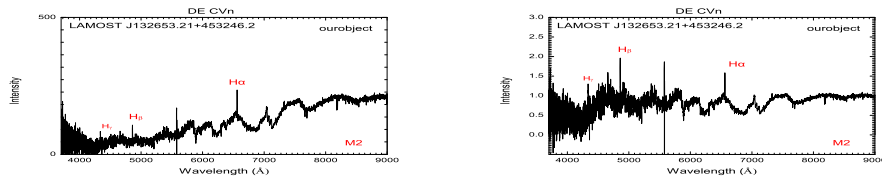
(e) LAMOST J090708.00+264440.2?

(f) LAMOST J224355.17+293647.4

Fig. 3. Examples of LAMOST spectra normalized to their continuum for stars with only one single spectrum from CSS, Kepler and LINEAR surveys. Some of them show obvious emissions in the Ca ii H&K, H$_\delta$, H$_\gamma$, H$_\beta$, H$_\alpha$ and Ca ii IRT lines.
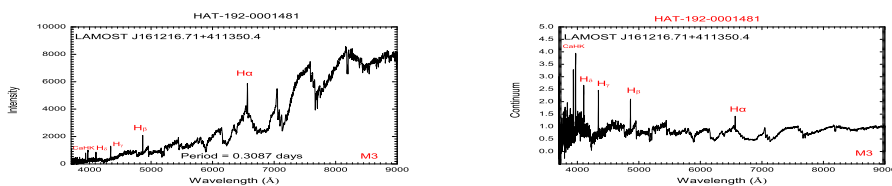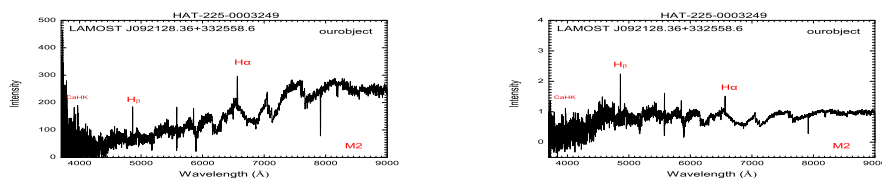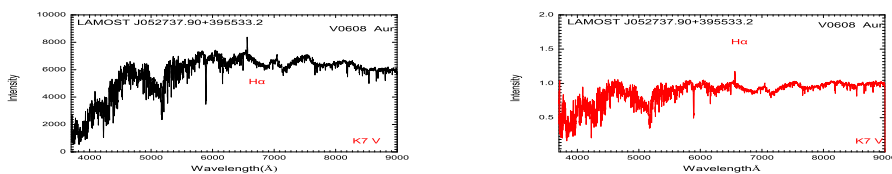
(g) LAMOST J220041.66+271513.5

(h) LAMOST J132653.21+453246.2

(i) LAMOST J161216.71+411350.4

(j) LAMOST J092128.36+332558.6

(k) LAMOST J052737.90+395533.2
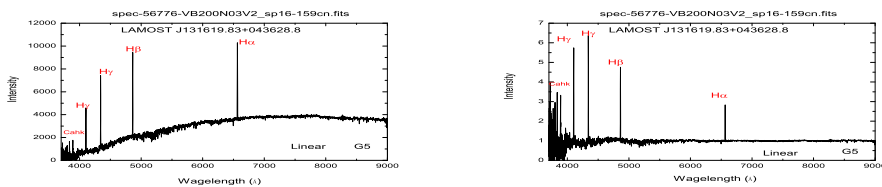
(ℓ) LAMOST J180947.64+490255.0

Fig. 3. (*continued*)

variable stars and eclipsing binaries observed in the LAMOST survey in Fig. 1, where different symbols and colors represent targets from different stellar surveys.

3. Analyses

The Ca ii K, H$_\alpha$, H$_\beta$, H$_\gamma$ and H$_\delta$ lines are useful chromospheric activity indicators (eg., Montes et al., 2001). In this section, we first present our statistical analyses on our sample of variable stars (including eclipsing binaries), we then describe the method of analyzing
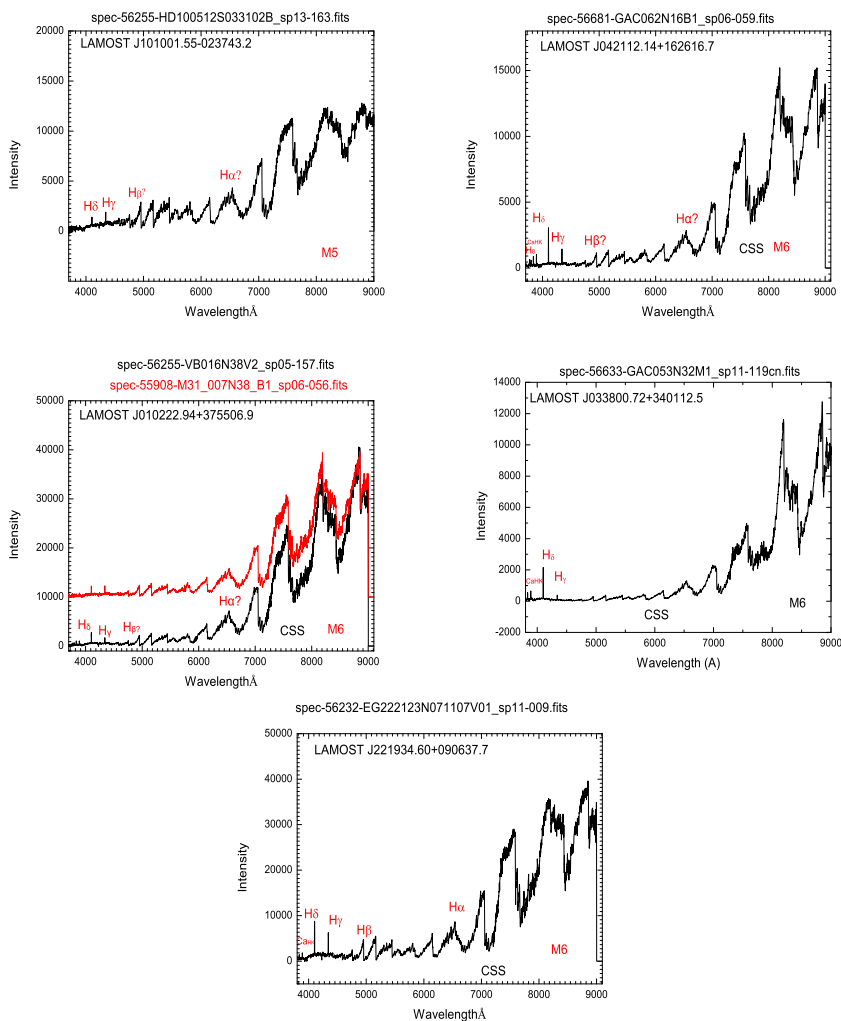
Fig. 4. LAMOST spectra of active stars, which show obvious emissions in the H_δ, or H_γ, or H_β. However there are no emissions in H_α line.

their chromospheric activity.

There are 11,469 periodic variables (5398 eclipsing binaries) observed in LAMOST survey. We analyzed their statistical distributions in terms of the number of stars with different spectral types and periods. Among them, there are 3443 variable stars (including 1467 eclipsing binaries) with at least two spectra. We plotted the number distribution vs. periods or spectral types for all stars and eclipsing binaries observed on LAMOST Survey in Fig. 2. The number of the eclipsing binaries of different spectral types are similar to that for other types of variable stars (RR Lyrae stars, and so on). The number of binaries with AFGK spectral types are larger than that for other spectral types. From the number distribution vs. the period, we found the number of eclipsing binaries with orbital period $<$ 1 day is larger than other stars and the number of eclipsing binaries with orbital period $>$ 1 day is less than other stars.

We used the program of West et al. (2004); 2011) to measure their equivalent widths of their chromospheric activity lines. We chose the wavelength regions of the continuum and lines regions that were used for studying SDSS spectra following Hilton et al. (2010) and West et al. (2004); 2011). This program calculated their EWs by integrating over regions around the center of these spectral lines and subtracting the mean background flux of two adjacent continuum regions (6555–6560 Å and 6570–6575 Å for H_α; 4840.0–4850.0 Å and 4875.0–4885.0 Å for H_β, 4310.0–4330.0 Å and 4350.0–4370.0 Å for H_γ; 4075.0–4095.0 Å and 4110.0–4130.0 Å for H_δ; and 3952.8–3956.0 Å and 3974.0–3976.0 Å for Ca ii K). The spectral types were determined by matching the observational spectra with models of standard stars (Wu et al., 2011; Luo et al., 2015). The uncertainties of the spectral types inferred from LAMOST spectra are from one to two subtypes (Yi et al., 2014) using the models of standand stars. We calculated the ratio between the height of the chromospheric activity line and its noise at the line center. We listed them in the column of "diff" in Table 3. To search and classify strong active stars using the H_α line, our criteria are similar to those of West et al. (2011) and Yi et al. (2014). That is, the EWs of the H_α line must be larger than 0 Å (for M star, larger than 0.75 Å) and larger than their uncertainties, and their heights of the H_α emission must be 3 times the noise (in other word, we impose that "diff" is above 3.) (Hawley et al., 2002; West et al., 2004). Moreover, we also visually inspected all candidate spectra of active variable stars and manually checked their magnetic activity spectral lines again. We define the EWs to be negative for absorption line and positive for emission line. Our criteria allow us to identify and discover targets with strong level of magnetic activity. Most of them are the accreting classical T
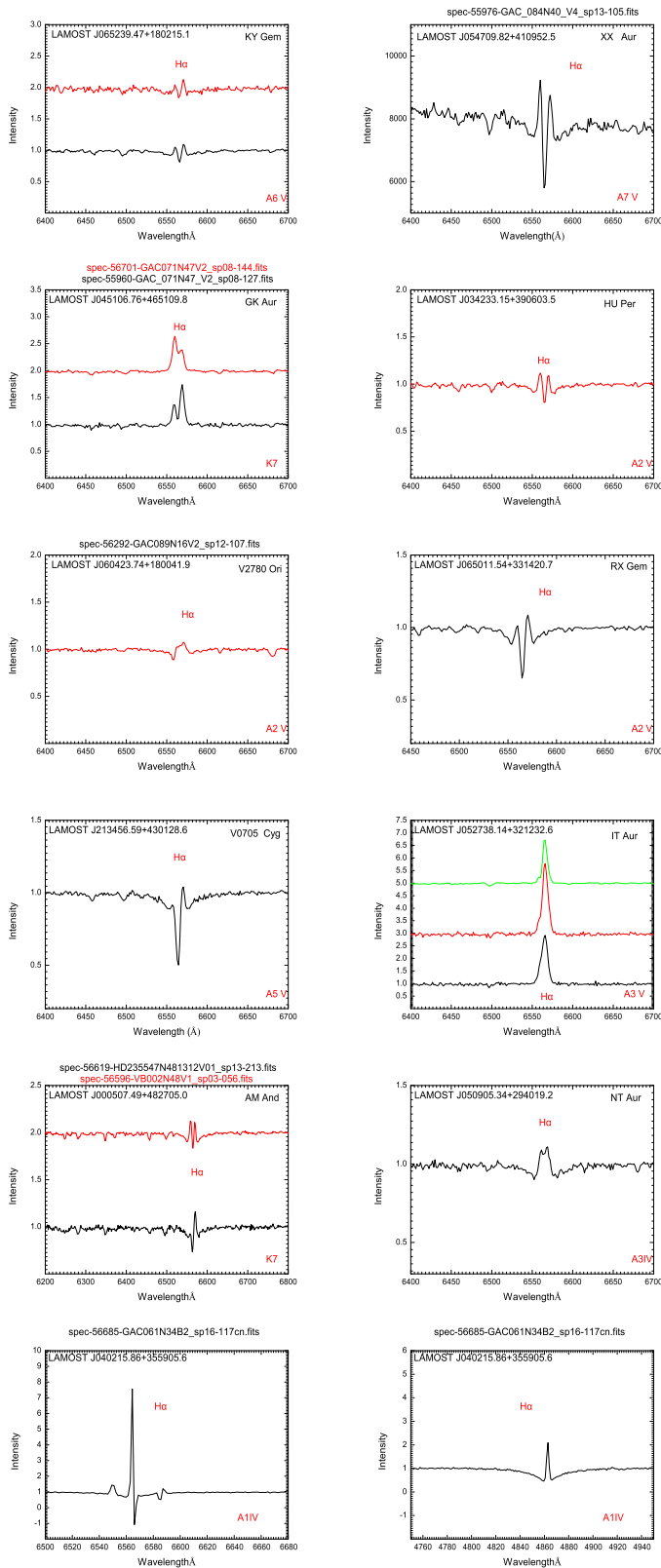
**Fig. 5.** LAMOST spectra of active stars, which show obvious core emissions in the H$_\alpha$ line.

Tauri stars (CTTS), as evidenced by the very large H$_\alpha$ EWs. We did not make use of the more accurate spectral subtraction technique (SST) to measure the emission EWs because we could not automate this process.

Therefore, large number of chromospherically active stars with FGK spectral types that have LAMOST DR2 spectra are missed from our detection. We only detect the most active since all active stars whose

Table 5
Spectral parameters of LAMOST targets with repeated spectra.

| No	LAMOST name	Source	Period d	Data	HJD d	Sp.T	Variation	Hα Å	Hβ Å	Hγ Å	Hδ Å
01	J000507.49+482705.0	AM And	8.850	2013-11-22		A3IV	v	-	14.317 ± 2.293	-	-
01	J000507.49+482705.0	AM And	8.850	2013-10-30		A3IV	v	-	15.214 ± 1.946	-	-
02	J010222.93+375506.9	CSS J010222.9+375506	236.183	2011-12-12	55,907	M6	v	-	-	16.342 ± 5.462	13.631 ± 0.771
02	J010222.94+375506.9	CSS J010222.9+375506	236.183	2011-11-23	56,254	M6	v	-	-	5.506 ± 0.007	16.974 ± 1.124
03	J012902.50-033744.4	CSS J012902.4-033744	0.3295	2014-1-9	56,666	M0	v	2.056 ± 0.036	-	-	-
03	J012902.50-033744.4	CSS J012902.4-033744	0.32953	2012-11-1	56,232	M0	v	2.345 ± 0.1	1.057 ± 0.013	-	-
03	J012902.50-033744.4	CSS J012902.4-033744	0.32953	2013-12-3	56,629	K7	v	1.771 ± 0.021	1.067 ± 0.02	-	-
03	J012902.50-033744.4	CSS J012902.4-033744	0.32953	2014-1-3	56,660	M0	v	1.647 ± 0.022	-	-	-
03	J012902.50-033744.4	CSS J012902.4-033744	0.32953	2013-10-29	56,594	M0	v	1.119 ± 0.045	-	-	-
04	J013159.85+294922.0	TT Tri	0.1396	2011-11-21		CV	v	-	-	-	-
04	J013159.85+294922.0	TT Tri	0.1396	2011-12-13		Non	v	22.536 ± 0.744	-	-	-
05	J014215.48+285850.5	CSS J014215.5+285850	5.1756	2012-1-13	55,939	M3	v	5.379 ± 0.345	4.544 ± 0.076	5.554 ± 0.014	-
05	J014215.48+285850.5	CSS J014215.5+285850	5.1756	2011-12-11	55,906	M3	v	1.836 ± 0.032	-	1.412 ± 0.097	2.200 ± 0.149
05	J014215.48+285850.5	CSS J014215.5+285850	5.1756	2012-1-4	55,930	M3	v	4.009 ± 0.021	-	-	-
06	J020202.37+193333.0	CSS J020202.3+193332	6.0904	2012-10-3	56,203	M0	v	2.701 ± 0.029	1.990 ± 0.104	1.879 ± 0.046	-
06	J020202.37+193333.0	CSS J020202.3+193332	6.0904	2012-10-3	56,203	M0	v	0.709 ± 0.031	-	-	-
07	J025637.95+245732.5	CSS J025637.9+245732	0.3639	2013-2-8	56,331	K7	n	1.414 ± 0.169	0.623 ± 0.018	-	-
07	J025637.95+245732.5	CSS J025637.9+245732	0.3639	2013-2-4	56,327	K7	n	1.522 ± 0.065	-	-	-
08	J030047.68+264213.6	CSS J030047.6+264213	3.0579	2013-2-8	56,331	K7	v	3.423 ± 0.077	-	-	-
08	J030047.68+264213.6	CSS J030047.6+264213	3.0579	2013-2-4	56,327	K3	v	1.497 ± 1E-3	-	-	-
09	J032619.81+310637.1	CSS J032619.8+310637	0.30066	2012-11-7	56,238	M0	v	25.032 ± 0.098	8.134 ± 0.158	1.793 ± 0.364	-
09	J032619.81+310637.1	CSS J032619.8+310637	0.30066	2012-1-11	55,937	Non	v	13.469 ± 0.751	-	-	-
10	J032842.43+302953.1	CSS J032842.4+302952	5.8266	2012-1-11	55,937	M4	n	32.406 ± 1.984	-	-	-
10	J032842.43+302953.1	CSS J032842.4+302952	5.8266	2013-2-14	56,337	M5	n	34.386 ± 0.246	21.275 ± 1.045	-	-
11	J034446.98+294835.5	CSS J034446.9+294836	2.9453	2013-1-28	56,320	M0	n	2.575 ± 0.058	1.694 ± 0.069	-	-
11	J034446.98+294835.5	CSS J034446.9+294836	2.9453	2013-1-24	56,316	K7	n	2.756 ± 0.088	3.628 ± 0.033	-	-
12	J034520.61+294657.2	CSS J034520.6+294657	1.1825	2013-11-22	56,618	M1	v	4.853 ± 0.065	7.933 ± 0.574	5.323 ± 0.193	8.353 ± 0.665
12	J034520.61+294657.3	CSS J034520.6+294657	1.18258	2013-1-28	56,320	M2	v	2.195 ± 0.178	-	-	-
12	J034520.61+294657.3	CSS J034520.6+294657	1.18258	2013-1-24	56,316	M3	v	4.091 ± 0.054	-	-	-
13	J034525.07+294352.9	CSS J034525.1+294352	13.8827	2013-1-24	56,316	M3	v	4.890 ± 0.058	1.560 ± 0.063	-	-
13	J034525.07+294352.8	CSS J034525.1+294352	13.8827	2013-11-22	56,618	M1	v	6.150 ± 0.087	6.487 ± 0.072	5.912 ± 0.125	25.111 ± 1.259
14	J034624.56+301608.7	CSS J034624.5+301608	9.1722	2013-12-3	56,629	M3	v	4.409 ± 0.118	6.852 ± 0.099	5.124 ± 0.063	4.508 ± 0.155
14	J034624.57+301608.9	CSS J034624.5+301608	9.1722	2013-1-28	56,320	M1	v	2.399 ± 0.12	-	-	-
15	J034740.96-024658.2	CSS J034740.9-024658	3.8798	2012-10-17	56,217	K3	n	3.936 ± 0.054	-	-	-
15	J034740.96-024658.2	CSS J034740.9-024658	3.8798	2012-10-17	56,217	K3	n	3.870 ± 0.003	-	-	-
⋮	⋮	⋮	⋮	⋮	⋮	⋮	⋮	⋮	⋮	⋮	⋮

This table is available in its entirety in machine-readable and Virtual Observatory (VO) forms in the online journal. A portion is shown here for guidance regarding its form and content.
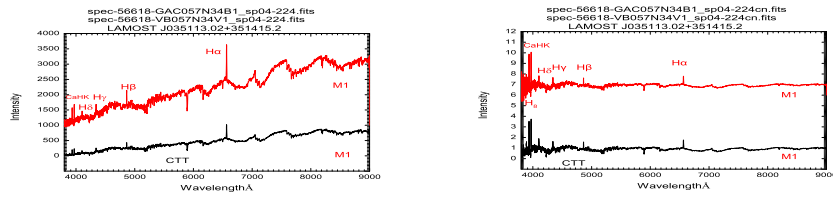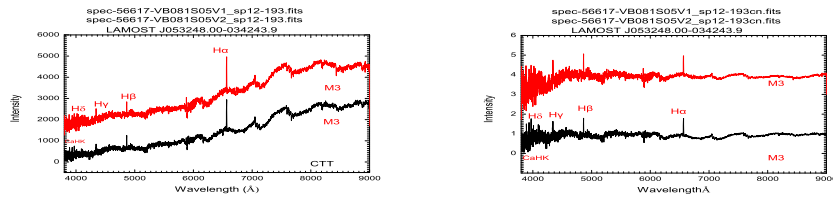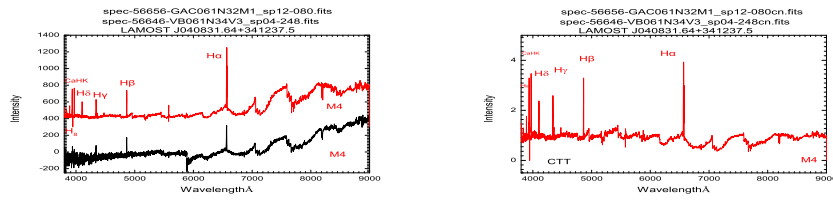
(a) LAMOST J035113.02+351415.2
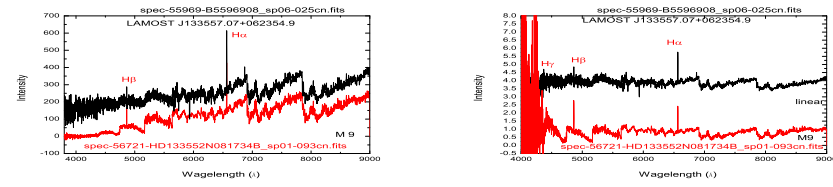
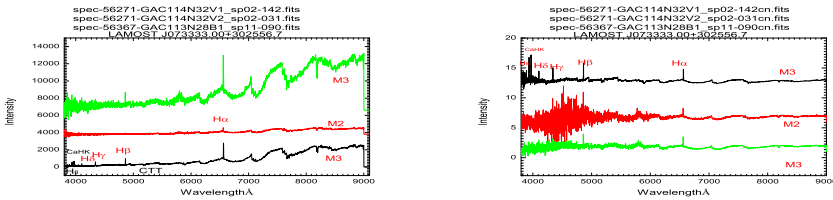(b) LAMOST J133557.07+062354.9
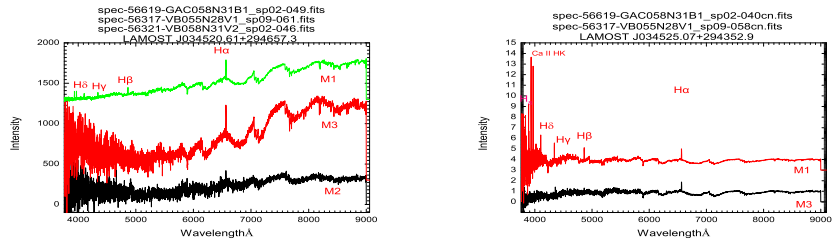
(c) LAMOST J034520.61+294657.3.epsgoodrepeated

(d) LAMOST J053248.00-034243.9

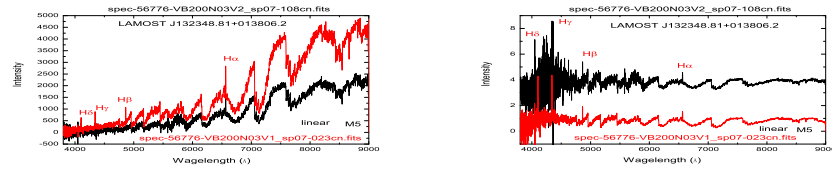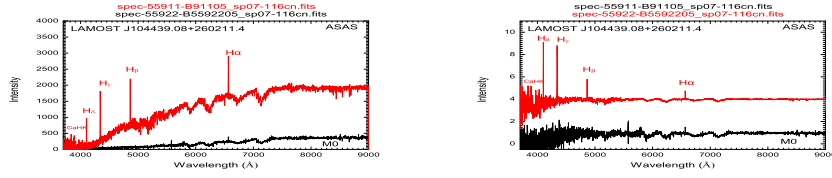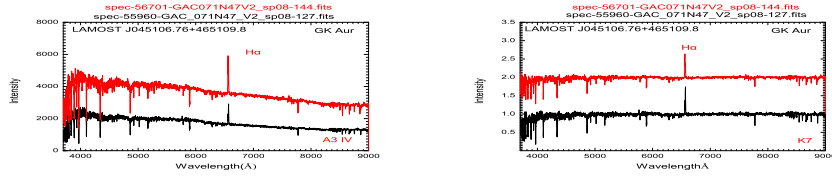(e) LAMOST J040831.70+341237.2

(f) LAMOST J073333.00+302556.7

Fig. 6. LAMOST repeated spectra normalized to their continuum for stars from CSS, LINEAR, Eclipsing catalogue and other surveys. Some of them show obvious emissions in the Ca ii H&K, H$_\delta$, H$_\gamma$, H$_\beta$, H$_\alpha$ and Ca ii IRT lines.
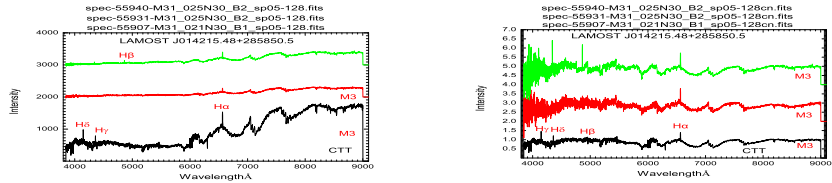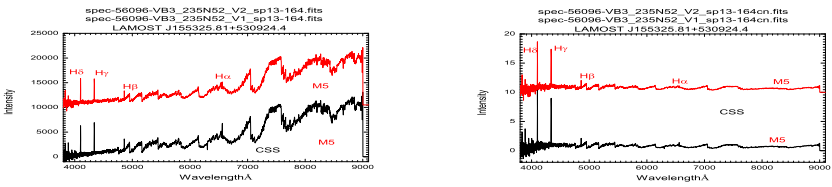
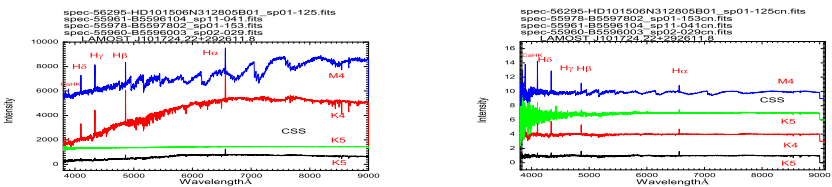(g) LAMOST J132348.81+013806.2

(h) LAMOST J104439.08+260211.4

(i) LAMOST J045106.76+465109.8

(j) LAMOST J014215.48+285850.5

(k) LAMOST J155325.81+530924.4

(ℓ) LAMOST J101724.22+292611.8

Fig. 6. (*continued*)

activity-sensitive lines are not filled in will be missed out. Frasca et al. (2016) analyzed LAMOST-Kepler stellar spectra with high signal to noise and by means of the spectral subtraction technique. In fact, all F, G, and early-K type stars with very prominent activity generally do not completely fill-in the H_α line (thus missed out by our

detection). In the future we will use more accurate and powerful techniques to recover also stars with lower level of activity. We listed some parameters (names, exposure time, EWs, the heights of emissions or depth of absorptions and the SN ratios.) of Ca ii K, H_α, H_β, H_γ and H_δ lines in Table 3. All parameters are available in electronic form (Cat5)
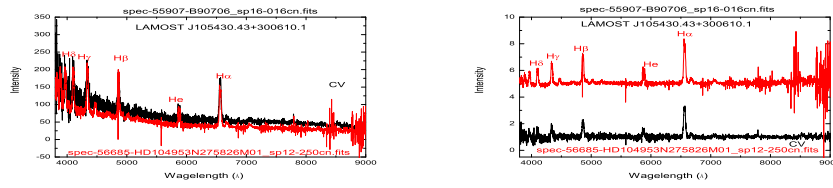
(a) LAMOST J065239.47+180215.1
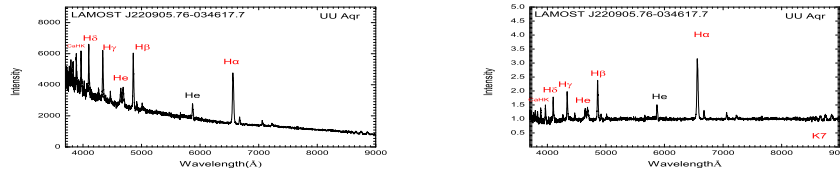
(b) LAMOST J054709.82+410952.5
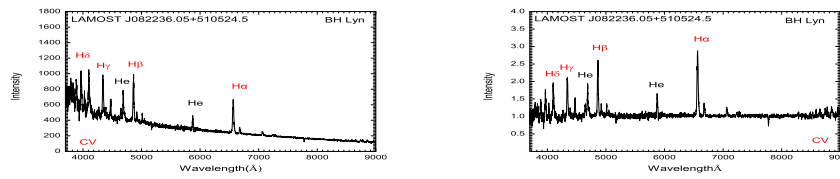
(c) LAMOST J052737.90+395533.2
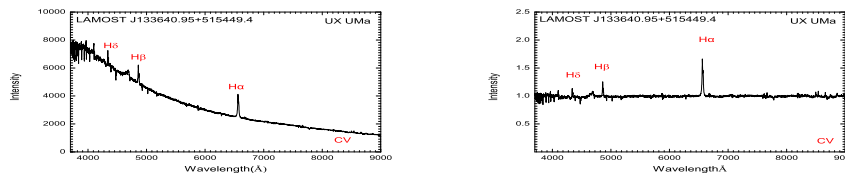
(d) LAMOST J045106.76+465109.8
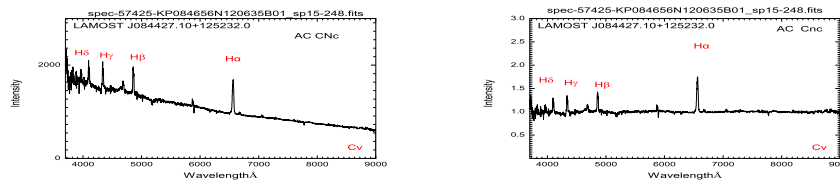
(e) LAMOST J064323.69+191452.9

41
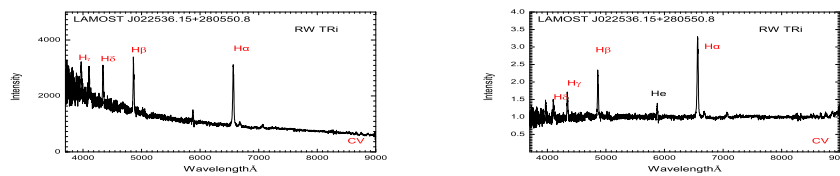
(f) LAMOST J064323.69+191452.9

Fig. 7. LAMOST spectra normalized to their continuum of cataclysmic variables. Most of them show obvious emissions in the Ca ii H&K, H_δ, H_γ, H_β, H_α and Ca ii IRT lines.
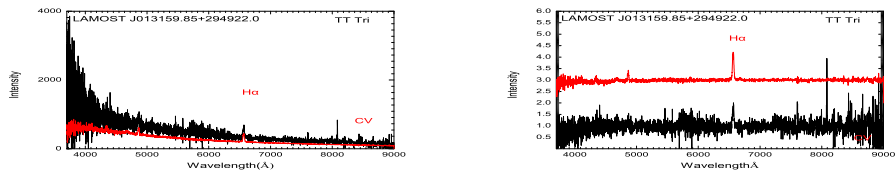
(g) LAMOST J065239.47+180215.1
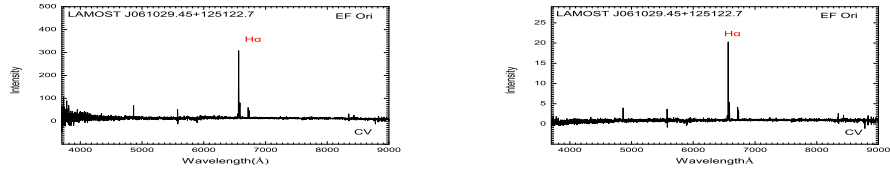
(h) LAMOST J053236.11-052301.0
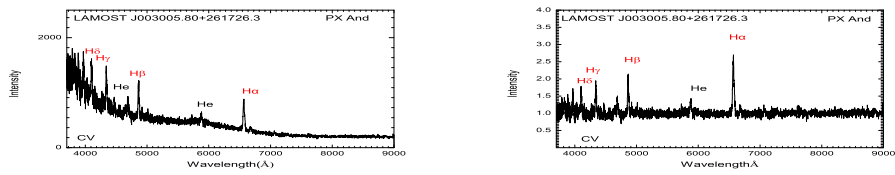
(i) LAMOST J105506.58+193157.9

(j) LAMOST J131714.28-050458.1

(k) LAMOST J142555.99+141210.1

(ℓ) LAMOST J151302.30+231508.6

Fig. 7. (*continued*)

Table 6
Spectral parameters of LAMOST CV targets.

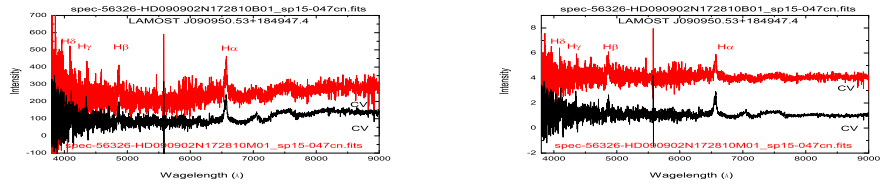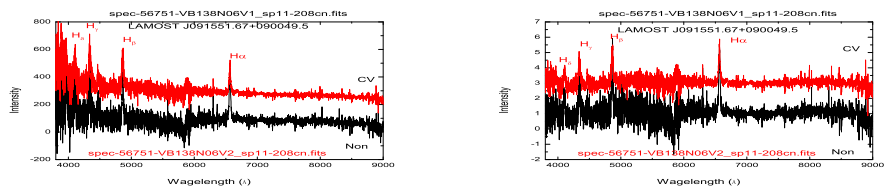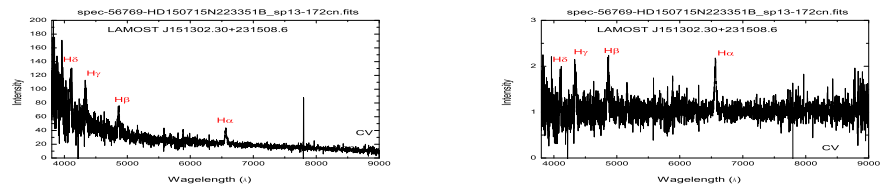| No	LAMOST name	Source	period d	Eclipsing	V	H$_\alpha$ Å	H$_\beta$ Å	H$_\gamma$ Å	H$_\delta$ Å	He 5706Å Å
01	J003005.80+261726.3	PX And	0.146353	Eclipsing	n	47.738 ± 0.868	22.343 ± 0.187	–	–	–
02	J013159.85+294922.0	TT Tri	0.139637	eclipsing	v	22.536 ± 0.744	–	–	–	–
02	J013159.85+294922.0	TT Tri	0.139637	eclipsing	v	–	–	–	–	–
03	J022536.15+280550.8	RW Tri	0.23188	eclipsing	n	57.773 ± 1.673	22.724 ± 0.416	–	–	–
04	J082236.05+510524.5	BH Lyn	0.155874	eclipsing	n	48.575 ± 1.595	28.981 ± 0.699	–	–	–
05	J082236.05+510524.5	BH Lyn	0.155874	eclipsing	n	47.834 ± 1.554	31.258 ± 1.158	21.414 ± 0.294	17.553 ± 0.323	10.702 ± 0.488
06	J084427.10+125232.0	AC Cnc	0.300477	eclipsing	n	22.379 ± 0.269	9.479 ± 0.010	–	–	–
07	J090950.53+184947.4	GY Cnc	0.175442	eclipsing	v	64.431 ± 3.409	50.183 ± 8.957	–	7.957 ± 2.698	–
07	J090950.53+184947.4	GY Cnc	0.175442	eclipsing	v	88.829 ± 1.379	38.984 ± 4.986	14.428 ± 3.892	7.105 ± 3.182	–
08	J091551.67+090049.5	GZ Cnc		noeclipsing	v	107.671 ± 1.571	122.196 ± 8.896	41.994 ± 16.336	25.473 ± 1.927	–
08	J091551.67+090049.5	GZ Cnc		noeclipsing	v	82.459 ± 3.089	80.579 ± 4.181	45.246 ± 6.104	20.645 ± 1.555	–
09	J105430.43+300610.1	SX LMi		noeclipsing	v	137.391 ± 2.591	91.108 ± 11.738	46.673 ± 1.277	33.803 ± 2.397	29.893 ± 10.000
09	J105430.43+300610.1	SX LMi		noeclipsing	v	90.003 ± 0.757	40.821 ± 2.319	23.165 ± 3.365	12.156 ± 3.094	17.319 ± 2.325
10	J133640.92+515449.6	UX UMa	0.19667	eclipsing	v	20.034 ± 1.444	4.041 ± 0.360	–	–	–
10	J133640.95+515449.4	UX UMa	0.19667	eclipsing	v	16.031 ± 0.351	3.559 ± 0.036	–	–	–
11	J151302.30+231508.6	NY Ser-		noeclipsing	n	34.072 ± 1.798	29.661 ± 1.869	19.882 ± 6.508	15.134 ± 3.916	-
12	J220905.76–034617.7	UU Aqr	0.16358	eclipsing	n	60.591 ± 16.229	26.622 ± 1.132	–	–	–

This table is available in its entirety in machine-readable and Virtual Observatory (VO) forms in the online journal. A portion is shown here for guidance regarding its form and content.

in the online version of the journal. Cat5 lists the EWs of our objects in these chromospheric activity lines.

4. Chromospherically active stars

4.1. Chromospheric activity

Among the variable star spectra, we found 447 active spectra for 316 active stars (including 178 eclipsing binaries). We identified for the first time 285 candidate chromospheric active stars from LAMOST spectra whereas 31 stars were already known to be active (Olson and Etzel, 2015; Wils et al., 2010; Hoard and Szkody, 1997). We listed part of the catalogue of the active stars in Table 4. The catalogue for all active stars is also available electronically in the online version (cat5). The table includes the name of each star, observation time, exposure time, spectral type, photometric period, EWs of the H$_\alpha$ and H$_\beta$ emission lines and their uncertainties. In order to show the observed spectra in different time, we normalized the spectra of the example active stars. In Fig. 3, we plotted some examples LAMOST spectra normalized to their continuum (such as LAMOST J142555.99+141210.1, LAMOST J220041.66+271513.5, LAMOST J131714.28–050458.1, LAMOST J025217.58+361648.1, LAMOST J104439.08+260211.4, LAMOST J131619.83+043628.8, LAMOST J104439.08+260211.4). We marked their chromospheric activity indicators in the subfigures. There are prominent emissions in many active stars. For some stars, there are no emissions in H$_\alpha$ line, such as LAMOST J010222.93+375506.9, LA-MOST J033800.72+340112.5, LAMOST J042112.14+162616.7, and LAMOST J101001.55–023743.2. However there are emission in H$_\beta$ or H$_\delta$ lines. We plotted these spectra in Fig. 4. For instance, we note that the emissions of H$_\alpha$ line might be deleted as cosmic ray by the LAMOST data processing pipeline. There are also 12 objects with some emission in the core of the H$_\alpha$ spectral line. We plotted them in Fig. 5, where the repeated spectra of four objects show chromospheric activity variability.

4.2. Chromospheric activity variability

Among 447 spectra of 316 very active stars, we investigated the spectral variability. We found 86 active stars (including 44 eclipsing binaries) with repeated spectra. We listed the stars and their parameters in Table 5. We determine the chromospheric variability using the difference between the maximum and minimum EWs of the H$_\alpha$ line. According to our criteria chromospheric variability is detected when this difference is larger than 3 times the corresponding uncertainty. This method is similar to that for studying the variability of chromospheric activity of M stars (Zhang et al., 2016). We found 68 of the 86 active stars (including 34 eclipsing binaries) showing chromospheric variations. In Fig. 6, we plotted some examples of LAMOST repeated spectra for active stars with chromospheric activity variability. We listed these stars and their parameters in Table 5. We need further observations to better characterize their variability properties.

5. Cataclysmic variable stars

Cataclysmic variable (CV) stars are close binary stars, where mass is transferred from a main-sequence star (primary component) to a white dwarf (secondary component) via an accretion disc (Hellier, 2001; Giovannelli, 2008). There are usually emission lines in their spectra showing strong hydrogen and helium emissions. Szkody et al. (2002); 2011) detected cataclysmic variables (CVs) from the Sloan Digital Sky Survey. The LAMOST spectra survey provides a rich database for studying CVs. Wei et al. (2013) used a novel outlier detection method to detect unusual and rare spectra from large spectral survey data sets, likely belonging to CV and Carbon stars. Among the periodic variable stars observed in LAMOST survey, there are 12 CV stars, with the star TT Tri having its first spectroscopic observation. We plotted the spectra of these 12 CV stars in Fig. 7 and list their parameters in Table 6. In the spectrum of TT Tri, we detected emissions in H$_\alpha$ and H$_\beta$ lines. There are 6 stars having repeated spectra, which show variations in the EWs of these spectral lines (see Table 6 and Fig. 7). The ongoing LAMOST surveys will certainly detect more cataclysmic variables in the future.
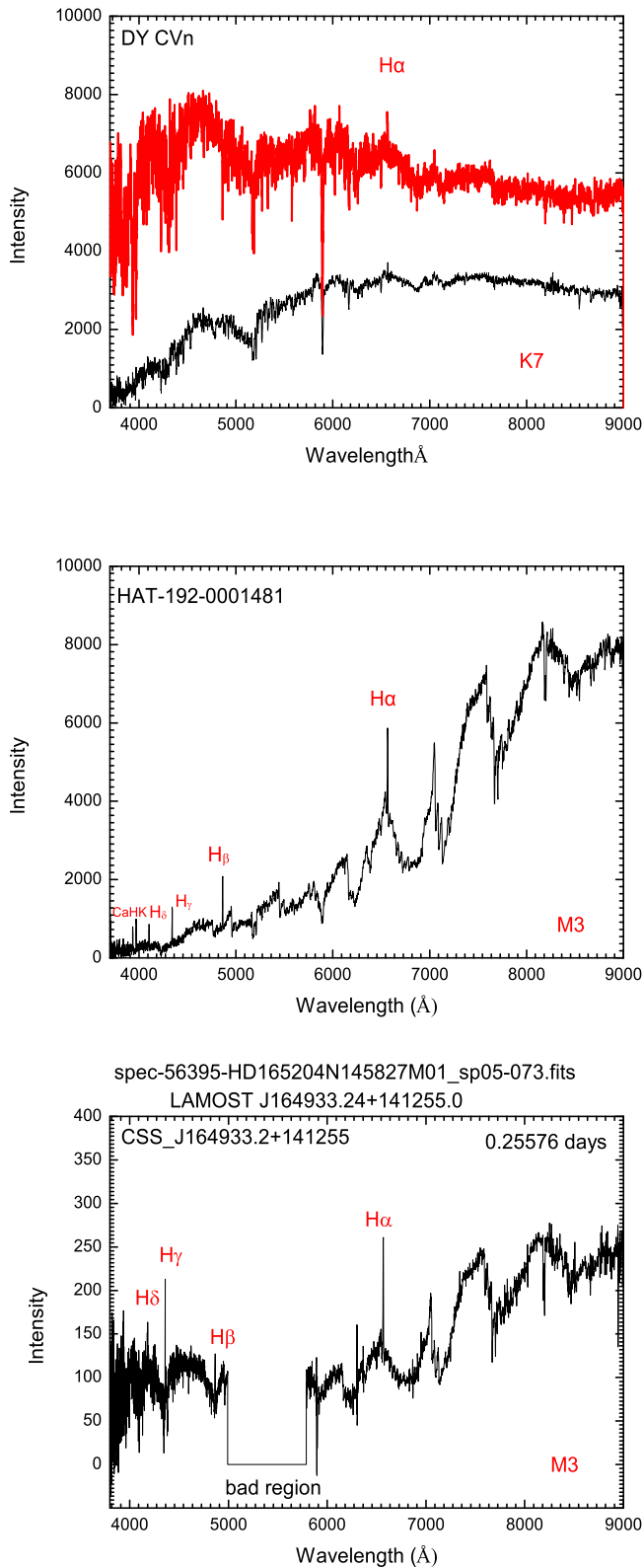
Fig. 8. LAMOST spectra of three eclipsing binaries, which show emissions in the H_α line.

6. Follow-up observations and modeling of some LAMOST targets

We have selected some interesting targets from LAMOST survey according to their orbital periods and chromospheric activity intensities. We plan to characterize them with the photometric follow-up monitoring and modeling. For the stars analysed in the present paper we used the 60-cm telescope at Xinglong Station of the National Astronomical Observatories of China (NAOC) (Lu et al., 2016), the Southeastern Association for Research in Astronomy (SARA KP) 90-cm telescope located at Kitt Peak National Observatory, SARA 1-m telescope (Jacobus Kapteyn Telescope, SARA RM) at the observatory del Roque de los Muchachos, La Palma, Spain (Keel et al., 2017). The effective field of view of the CCD is about 15–17 × 15-17 square arcmin. Each telescope has a 1024 × 1024 (or binned to 1024 × 1024) pixel CCD system for optical imaging, and with the standard Johnson UBVRI filter system for Xinglong 60-cm telescope, and Bessel system for SARA RM and KP telescopes. The dates of observations are between the April and June, 2016. In the present paper, we only show the results for three targets (DY CVn, HAT-192-0001481, and LAMOST J164933.24 + 141255.0), and we will extend the photometric follow-up study to other targets. DY CVn was discovered to be an eclipsing binary from ROTSE All-Sky Surveys by Akerlof et al. (2000) and from the HATNet survey by Hartman et al. (2011). Qu et al. (2017) obtained photometric VRI light curves with a gap and obtained their orbital parameters. HAT-192-0001481 was discovered to be a periodic variable star by CSS (Drake et al., 2014a) and HATNET survey (Hartman et al., 2011). LAMOST J164933.24 + 141255.0 was also discovered as an eclipsing binary by CSS survey (Drake et al., 2014a). Pribulla et al. (2012) included this star in their project to discover exoplanets.

6.1. Short period binaries observed in the LAMOST spectral survey

Among the most active stars in the LAMOST survey, 102 (88 eclipsing binaries) of them have rotation periods less than 0.5 days, and 38 (36 eclipsing binaries) of them have periods between 0.5 days and 1 days, and 169 (54 eclipsing binaries) of them have period greater than 1 days. We determined the spectral types for 16 short period binary candidates with period less than 0.25 days (12 of them less than 0.22 days). It is important for us to understand the reason of orbital period cut off of eclipsing binary and stellar theory of stellar and binary evolution (Jiang et al., 2012). There are 3 eclipsing binaries with M spectral type. More and more researchers are interested in ultra short period M eclipsing binary (Drake et al., 2014b; Lohr et al., 2013). There are 7 eclipsing binaries with repeated spectra, and 5 of them show chromospheric variations. More full-phase coverage multi-filter photometric observations are needed to improve their binary models. We present our work on three eclipsing binaries in next section.

6.2. Photometric observations of three short period binaries

Among the short-period binaries with late spectral type components and evidence of chromospheric activity, we selected three objects (DY CVn, HAT-192-0001481, and LAMOST J164933.24 + 141255.0) for follow-up photometric observations and modeling. We plotted their LAMOST spectra in Fig. 8. We listed their parameters in Table 7 . We carried out the follow-up photometric multi-filters CCD observations of DY CVn On April 16, and 23, 2016 using the 60-cm telescope (Lu et al., 2016) at Xinglong Station of NAOC with Johnson *VRI* filters. The exposure times are 120–150 s, 90 s and 50–60 s in V, R, I filters,

Table 7

Relevant parameters of DY CVn and HAT-192-0001481, their check and comparison stars, coordinates and magnitudes.

Targets	Name	Coordinates	Mag_J	Mag_H	Mag_K	Reference
Variable	DY CVn	13:47:26.90; +17:18:24.0	11.270	10.943	10.880	[1] [2]
Comparison	GSC 01460-00003	13:47:03.82; +17:22:05.4	11.353	10.962	10.905	[1] [3]
Check	GSC 01460-00206	13:47:28.62; +17:19:09.7	11.714	11.224	11.127	[1] [3]
Variable	HAT-192-0001481	16:12:16.68; +41:13:50.9	10.508	9.965	9.679	[1] [2]
Comparison	star J161214.57 + 410921.1	16:12:14.57; +41:09:21.1	-	-	-	[1] [3]
Check	2MASS J161247.38 + 411402.8	16:12:47.38; +41:14:02.8	-	-	-	[1] [3]
Variable	LAMOST J164933.24 + 141255.0	16:49:33.24; +14:12:55.0	15.830r	14.754i	14.031i	[1] [2]
Comparison	TYC 974-890-1	16:49:13.66; +14:07:52.0	10.575	10.267	10.225	[1] [3]
Check	2MASS J164923.74 + 141104.1	16:49:23.74 +14:11:04.1	-	-	-	[1] [3]

1. Cutri et al. 2003; 2. Samus et al. 2003; 3. Morrison et al. 2001.

respectively. We carried out the observations of HAT-192-0001481 on May 19, and 23, 2016 using the SARA 90-cm telescope (Keel et al., 2017) located at Kitt Peak National Observatory with Bessel *BVRI* filters with exposure times of 60 s, 45 s, 30 s, and 30 s, respectively. We carried out the observations of LAMOST J164933.24 + 141255.0 on June 7, 2016 using the 60-cm telescope at Xinglong Station, and on June 11, in 2016 using the *1-m* SARA RM telescope (Keel et al., 2017), and June 18, 2016 using the 90-cm SARA KP telescope. We used the Bessel *RI* filters with exposure times of about 120 s.

We reduced all our CCD images using the IRAF Package. The procedure included bias subtraction, flat-field division, cosmic ray removal, and aperture photometry. We chose comparison and check stars near the targets in the same field. The magnitude differences between our objects and their corresponding comparison star are shown in Figs. 9, and listed in Table 8. We fit our light curve using a polynomial function with the least square method and obtained several new light minimum times and their uncertainties (Kwee and van Woerden, 1956; Nelson 2007). We listed the new minima and corresponding uncertainties in Table 9. We obtained updated linear ephemeris as follows:

$$DYCVn \ : \ Min. \ I = HJD2452337.7617(5)$$
$$+ \ 0^d.24594930(4)E$$
$$HAT - 192 - 1481 \ : \ Min. \ I = HJD2453853.9056(6)$$
$$+ \ 0^d.30873908(6)E$$
$$J164933.2 + 141255 \ : \ Min. \ I = HJD2457547.197(7) + 0^d.2555(2)E$$

The orbital phases of these three eclipsing binaries are calculated using these new ephemerides.

6.3. Photometric modeling of three active eclipsing binaries

We used our new CCD photometric multi-color light curves to obtain the orbital solutions for DY CVn, and HAT-192-0001481 using the 2003 version of the WD program (Wilson, 1979; 1990). Because the light curves of LAMOST J164933.24 + 141255 are quite irregular owing to short timescale activity, we did not obtain its orbital parameters. We chose their gravity-darkening coefficients as $g_1 = g_2 = 0.32$ (Lucy, 1967) and their bolometric albedos $A_1 = A_2 = 0.5$ (Rucinski, 1973). The resulting effective temperature of the corresponding primary was 4505 ± 131 K for DY CVn, and 3403 ± 131 K for HAT-192-0001481. We determined the limb-darkening of primary component based on its temperature according to the JHK magnitudes (Van Hamme, 1993). For the limb-darkening of secondary component, we set its initial value according to the temperature of the secondary component which was estimated to be about 200 K lower than the

primary component. Then we have adjusted the limb darkening of the secondary based on the result of the secondary temperature determined by the WD program. We used Mode 3 (appropriate for contact binaries) of the Wilson-Devinney code for DY CVn, and Model 2 (appropriate for detached binaries) for HAT-192-0001481.

Because LAMOST did not obtain the radial velocity curves to get spectroscopic mass ratio q = M_2/M_1 (the secondary divided by the primary), we used the relation of a mass ratio and the weighted sum of squares of residuals to search the reasonable results. We then plot the fitting residual $\Sigma (O - C)_i^2$ as a function of the mass ratio q in Fig. 10. We chose the *q* value which produced the least fitting residual to be the mass ratio for each binary system. Using the procedures described in our previous papers (e.g., Zhang et al., 2015), we obtained the orbital parameters (orbital inclination, temperature of the secondary component, dimensionless gravitational potentials of the primary and secondary component (Ω_1 and Ω_2), and listed them in Table 10. We also plotted the theoretical and observed light curves of DY CVn and HAT-192-0001481 and only the observed light curves of LAMOST J164933.24 + 141255.0 in Fig. 9, and the corresponding configurations at phases 0.25 or 0.75 in Fig. 11. For DY CVn, our results are similar to the orbital inclination (88°), the mass ratio (1.3), and the luminosity ratio (about 0.4) derived by Qu et al. (2017). As can be seen from Fig. 8, the emissions of the H_α line suggest strong magnetic activities. For HAT-192-0001481, there is a remarkable asymmetry in its light curves (The Max.I is higher than Max.II at phase 0.75). We explained it by assuming the presence of one starspot on the primary component. The starspot parameters are also listed in Table 9.

6.4. The first flare observed in LAMOST J164933.24 + 141255.0

Many short-period eclipsing binaries observed in LAMOST survey show strong chromospheric activities with the H_α emissions above continuum. We are interested in photometric follow-up monitoring of short period (less than 0.3 days) eclipsing binaries with M spectral type and strong chromospheric activities among the LAMOST targets. LAMOST J164933 + 141255 is the first star that we photometrically monitored. Although there is a bad region in the spectra of LAMOST J164933.24 + 141255.0, we still found it is strongly chromospherically active. Flares are the sudden and interesting random events of releasing magnetic energy above stellar atmosphere. It is possible to detect them in chromospheric active eclipsing binaries by means of photometric follow-up monitoring. Fortunately we detected possibly the first flare event in LAMOST J164933.24 + 141255.0 on June 11, 2016. We calculated the flare duration to be 2.9469 h. It took about 0.179 h to reach its peak. The duration covered about half of the orbital period. The
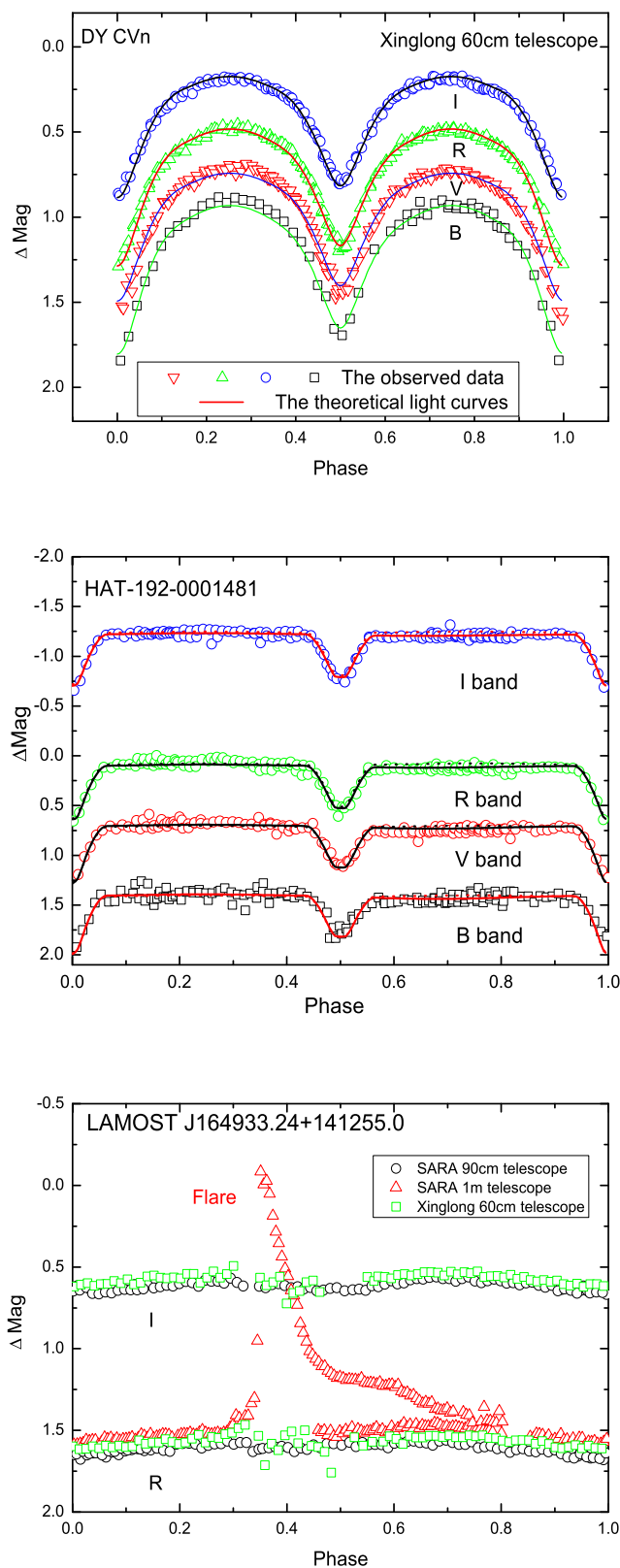
maximum amplitude of the flare was about 1.482 mag in R filter (Fig. 12). The discovery of the flare event on LAMOST J164933.24 + 141255.0 is consistent with it strong chromospheric emission. Similar flare events were also found in other eclipsing binaries with M spectral type, such as AD Leo (Hawley and Pettersen, 1991), CM Dra (Kozhevnikova et al., 2004), CU Cnc (Qian et al., 2012), DV Psc (Pi et al., 2014), NSVS 06,550,671 (Dimitrov and Kjurkchieva, 2010), NSVS 07,453,183 (Zhang et al., 2014), V405 And (Vida et al., 2009), YZ CMi (Kowalski et al., 2016) and YY Gem (Doyle et al., 1990). However, the flare that we detected on LAMOST J164933.24 + 141255.0 is among the largest detected on low-mass eclipsing binaries with M spectral type. We will continue to carry out a photometric follow-up observations of other active LAMOST targets.

7. Conclusions

Using different photometric catalogs of periodic variables stars, we selected a sub-sample having stellar spectra in the LAMOSR DR2 survey.

1. We found 15,955 stellar spectra for 11,469 periodic variable stars (including 5398 eclipsing binaries) from the LAMOST survey.

2. We found 316 active variable stars (178 eclipsing binaries) with strong chromospheric activities.

3. We obtained the orbital and starspot parameters for two short-period eclipsing binaries with LAMOST spectra (DY Cvn and HAT-192-0001481).

4. We detected the first flare event in LAMOST J164933.24 + 141255.0 with an amplitude of 1.48 mag in R band.

Using our method, we detect only very active M stars. We measured a lower limit on the activity level, as well as the sample of periodic variable stars considered in the present study is incomplete. Therefore it becomes meaningless to search for any correlation of the activity level measured by us in a number of activity-sensitive lines with spectral type, binary, orbital period. We will discuss them in the future.

Fig. 9. Observed and theoretical light curves of DY CVn and HAT-192-0001481, and observed light curves of LAMOSTJ164933.24 + 141255.0.

Table 8

New BVRI photometric data of DY CVn, HAT-192-0001481 and LAMOST J164933.24 + 141255.0.

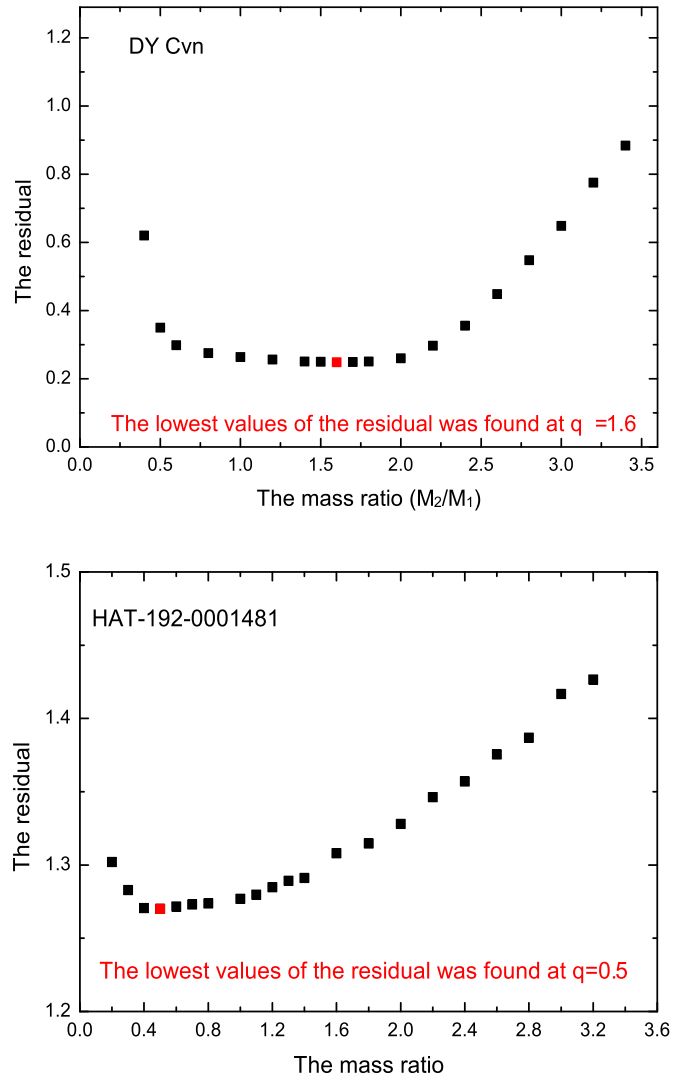| Star name	B filter		V filter		R filter		I filter		Telescope
	HJD d	Δ mag	HJD d	Δ mag	HJD d	Δ mag	HJD d	Δ mag	
DY CVn	2457494.9899	1.025	2457494.9912	0.764	2457494.9922	0.545	2457494.9888	0.215	60 cm telescope
DY CVn	2457494.9941	0.910	2457494.9954	0.737	2457494.9964	0.505	2457494.9930	0.205	60 cm telescope
DY CVn	2457494.9982	0.987	2457494.9995	0.752	2457495.0005	0.526	2457494.9972	0.219	60 cm telescope
DY CVn	2457495.0023	0.919	2457495.0036	0.735	2457495.0045	0.498	2457495.0012	0.172	60 cm telescope
DY CVn	2457495.0063	0.901	2457495.0076	0.714	2457495.0086	0.477	2457495.0053	0.189	60 cm telescope
DY CVn	2457495.0104	0.927	2457495.0117	0.728	2457495.0126	0.475	2457495.0093	0.175	60 cm telescope
DY CVn	2457495.0144	0.930	2457495.0157	0.723	2457495.0167	0.491	2457495.0134	0.179	60 cm telescope
DY CVn	2457495.0185	0.948	2457495.0198	0.729	2457495.0207	0.514	2457495.0174	0.171	60 cm telescope
DY CVn	2457495.0225	0.919	2457495.0238	0.752	2457495.0248	0.514	2457495.0215	0.197	60 cm telescope
DY CVn	2457495.0266	0.944	2457495.0279	0.785	2457495.0288	0.532	2457495.0255	0.207	60 cm telescope
DY CVn	2457495.0306	0.964	2457495.0319	0.791	2457495.0329	0.561	2457495.0296	0.248	60 cm telescope
DY CVn	2457495.0346	0.981	2457495.0359	0.809	2457495.0369	0.579	2457495.0336	0.248	60 cm telescope
DY CVn	2457495.0389	1.063	2457495.0404	0.861	2457495.0413	0.623	2457495.0376	0.277	60 cm telescope
DY CVn	2457495.0434	1.123	2457495.0449	0.905	2457495.0458	0.661	2457495.0421	0.299	60 cm telescope
DY CVn	2457495.0478	1.168	2457495.0493	0.964	2457495.0503	0.710	2457495.0466	0.332	60 cm telescope
DY CVn	2457495.0523	1.215	2457495.0538	1.061	2457495.0548	0.785	2457495.0510	0.410	60 cm telescope
DY CVn	2457495.0571	1.340	2457495.0587	1.155	2457495.0596	0.930	2457495.0555	0.463	60 cm telescope
DY CVn	2457495.0617	1.519	2457495.0632	1.316	2457495.0641	1.058	2457495.0604	0.567	60 cm telescope
DY CVn	2457495.0662	1.638	2457495.0677	1.423	2457495.0686	1.164	2457495.0649	0.671	60 cm telescope
DY CVn	2457495.0707	1.842	2457495.0721	1.555	2457495.0731	1.277	2457495.0694	0.805	60 cm telescope
...	...	...	...	...	...	...	...	...	...
HAT-192-0001481	2457525.6388384	1.428	2457525.6359940	.769	2457525.6366304	0.109	2457525.6372804	−1.239	SARA90 cm telescope
HAT-192-0001481	2457525.6424684	1.452	2457525.6396440	.710	2457525.6402804	0.082	2457525.6409103	−1.235	SARA90 cm telescope
HAT-192-0001481	2457525.6461083	1.426	2457525.6432739	.706	2457525.6439103	0.113	2457525.6445503	−1.208	SARA90 cm telescope
HAT-192-0001481	2457525.6497583	1.394	2457525.6469239	.728	2457525.6475603	0.123	2457525.6481903	−1.223	SARA90 cm telescope
HAT-192-0001481	2457525.6533983	1.394	2457525.6505639	.730	2457525.6512002	0.118	2457525.6518403	−1.211	SARA90 cm telescope
HAT-192-0001481	2457525.6570583	1.402	2457525.6542238	.725	2457525.6548602	0.091	2457525.6555002	−1.216	SARA90 cm telescope
HAT-192-0001481	2457525.6606982	1.383	2457525.6578738	.701	2457525.6585102	0.098	2457525.6591402	−1.161	SARA90 cm telescope
HAT-192-0001481	2457525.6643482	1.328	2457525.6615138	.712	2457525.6621502	0.067	2457525.6627901	−1.199	SARA90 cm telescope
HAT-192-0001481	2457525.6679782	1.384	2457525.6651438	.738	2457525.6657801	0.102	2457525.6664201	−1.204	SARA90 cm telescope
HAT-192-0001481	2457525.6716281	1.411	2457525.6687937	.699	2457525.6694301	0.122	2457525.6700701	−1.199	SARA90 cm telescope
HAT-192-0001481	2457525.6752581	1.400	2457525.6724337	.744	2457525.6730701	0.089	2457525.6737001	−1.189	SARA90 cm telescope
HAT-192-0001481	2457525.6789181	1.458	2457525.6760736	.738	2457525.6767200	0.121	2457525.6773600	−1.185	SARA90 cm telescope
HAT-192-0001481	2457525.6828880	1.360	2457525.6799136	.733	2457525.6805500	0.120	2457525.6813100	−1.197	SARA90 cm telescope
HAT-192-0001481	2457525.7863971	1.439	2457525.6838336	.704	2457525.6844700	0.130	2457525.6851000	−1.187	SARA90 cm telescope
HAT-192-0001481	2457525.7891571	1.393	2457525.7863127	.701	2457525.7869491	0.063	2457525.7875991	−1.235	SARA90 cm telescope
HAT-192-0001481	2457525.7929371	1.421	2457525.7899727	.675	2457525.7906091	0.078	2457525.7913890	−1.227	SARA90 cm telescope
HAT-192-0001481	2457525.7968870	1.415	2457525.7939126	.707	2457525.7945590	0.067	2457525.7953290	−1.234	SARA90 cm telescope
HAT-192-0001481	2457525.8009070	1.373	2457525.7980726	.686	2457525.7987090	0.058	2457525.7993490	−1.245	SARA90 cm telescope
HAT-192-0001481	2457525.8051970	1.367	2457525.8023726	.645	2457525.8030089	0.053	2457525.8036389	-1.266	SARA90cm telescope
...	...	...	...	...	...		...		...
J164933.24 + 141255.0					2457557.65442	1.614	2457557.65592	0.637	SARA90cm telescope
J164933.24 + 141255.0					2457557.65746	1.626	2457557.65897	0.626	SARA90cm telescope
J164933.24 + 141255.0					2457557.66051	1.631	2457557.66201	0.622	SARA90cm telescope
J164933.24 + 141255.0					2457557.66355	1.658	2457557.66507	0.642	SARA90cm telescope
...	...	...	...	...	...		...		
J164933.24 + 141255.0					2457558.33824	1.498			SARA 1m telescope
J164933.24 + 141255.0					2457558.33970	1.511			SARA 1m telescope
J164933.24 + 141255.0					2457558.34116	1.5			SARA 1m telescope
J164933.24 + 141255.0					2457558.34261	1.529			SARA 1m telescope
J164933.24 + 141255.0					2457558.34407	1.503			SARA 1m telescope
J164933.24 + 141255.0					2457558.34553	1.536			SARA 1m telescope
...	...	...	...	...	...	...	...	...	...

This table is available in its entirety in machine-readable and Virtual Observatory (VO) forms in the online journal. A portion is shown here for guidance regarding its form and content.

Table 9

Newly obtained minimum times of DY CVn, HAT-192-0001481 and LAMOST J164933.24 + 141255.0 in BVRI bands.

Name	HJD (B) d	HJD (V) d	HJD (R) d	HJD (I) d	HJD (average) d	Type
DY CVn			56986.2572 ± 0.0012	56986.2576 ± 0.0006	56986.2574 ± 0.0009	Primary
DY CVn			56986.0871 ± 0.0033	56986.0874 ± 0.0016	56986.0872 ± 0.0025	Secondary
DY CVn	57318.8683 ± 0.0008	57318.8687 ± 0.0005	57318.8688 ± 0.0005	57318.8686 ± 0.0008	57318.8686 ± 0.0007	Primary
DY CVn	57318.6963 ± 0.0004	57318.6959 ± 0.0008	57318.6959 ± 0.0006	57318.6959 ± 0.0005	57318.6960 ± 0.0006	Secondary
HAT-192-0001481	57525.8948 ± 0.0106	57525.8948 ± 0.0062	57525.8944 ± 0.0039	57525.8945 ± 0.0060	57525.8946 ± 0.0067	Secondary
HAT-192-0001481	57531.7589 ± 0.0497	–	57531.7602 ± 0.0046	57531.7598 ± 0.0015	57531.7596 ± 0.0186	Secondary
HAT-192-0001481	57531.9139 ± 0.0102	57531.9140 ± 0.0053	57531.9142 ± 0.0099	57531.9137 ± 0.0059	57531.9139 ± 0.0078	Secondary
J164933.24 + 141255.0	–	–	57547.1968 ± 0.0002	57547.1977 ± 0.0004	57547.1973 ± 0.0004	Primary
J164933.24 + 141255.0	–	–	57557.6797 ± 0.0026	-	57557.6797 ± 0.0026	Primary
J164933.24 + 141255.0	–	–	57557.9262 ± 0.0036	57557.9393 ± 0.0058	57557.93280 ± 0.0048	Primary
J164933.24 + 141255.0	–	–	57557.7812 ± 0.0046	57557.8028 ± 0.0016	57557.79201 ± 0.0032	Secondary

Note. Minimum times is that HJD minus 2,400,000 day.

Table 10

Orbital parameters of DY CVn and HAT-192-0001481.

Star Name	DY CVn	HAT-192-0001481
x_{1bolo}	0.532	0.286
x_{2bolo}	0.505	0.286
x_{1B}	0.944	0.655
x_{2B}	0.940	0.655
x_{1V}	0.795	0.622
x_{2V}	0.794	0.622
x_{1R}	0.658	0.516
x_{2R}	0.666	0.516
x_{1I}	0.532	0.409
x_{2I}	0.532	0.409
T_1 (K)	4505 a	3403 a
T_2 (K)	4368 ± 14	3331 ± 12
Ω_1	4.691 ± 0.007	4.937 ± 0.060
Ω_2	4.691 ± 0.007	4.342 ± 0.043
$q(m_2/m_1)$	1.600 ± 0.003	0.500 ± 0.050
$i(°)$	81.916 ± 0.145	87.867 ± 0.304
$L_1/(L_1 + L_2)(B)$	0.460 ± 0.002	0.701 ± 0.002
$L_1/(L_1 + L_2)(V)$	0.446 ± 0.002	0.695 ± 0.002
$L_1/(L_1 + L_2)(R)$	0.434 ± 0.001	0.687 ± 0.002
$L_1/(L_1 + L_2)(I)$	0.424 ± 0.001	0.683 ± 0.002
$r_1(pole)$	0.3159 ± 0.0007	0.2247 ± 0.0030
$r_1(point)$	–	0.2291 ± 0.0033
$r_1(side)$	0.3300 ± 0.0008	0.2267 ± 0.0031
$r_1(back)$	0.3613 ± 0.0011	0.2284 ± 0.0032
$r_2(pole)$	0.3940 ± 0.0007	0.1610 ± 0.0022
$r_1(point)$	–	0.1645 ± 0.0024
$r_2(side)$	0.4164 ± 0.0008	0.1621 ± 0.0023
$r_2(back)$	0.4448 ± 0.0011	0.1640 ± 0.0024
$Latitude_{spot1}$	–	90° a
$Longitude_{spot1}$	–	252.7 ± 10°
$Radius_{spot1}$	–	16.0 ± 0.4°
$Temperature_{spot1}$	–	3062 K ± 32 K
Σ	0.249	1.04

Parameters not adjusted in the solution are denoted by a mark "a". The spot latitude 90° means that spot center is on the equator of the component.
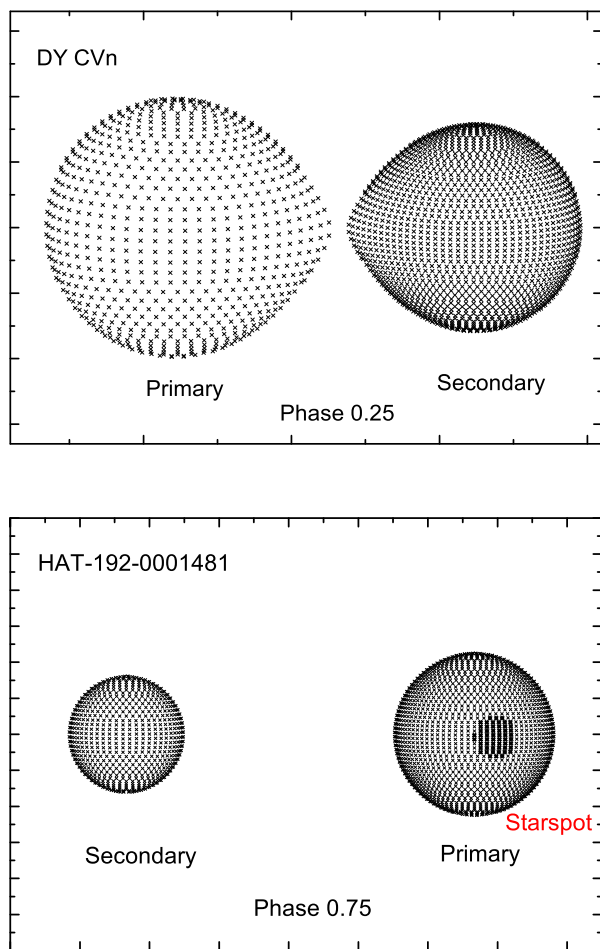
Fig. 10. Relationships between the residual Σ-q for DY CVn and HAT-192-0001481.

Fig. 11. Stellar and starspot configurations for DY CVn at phase 0.25 and HAT-192-0001481 at phase 0.75.
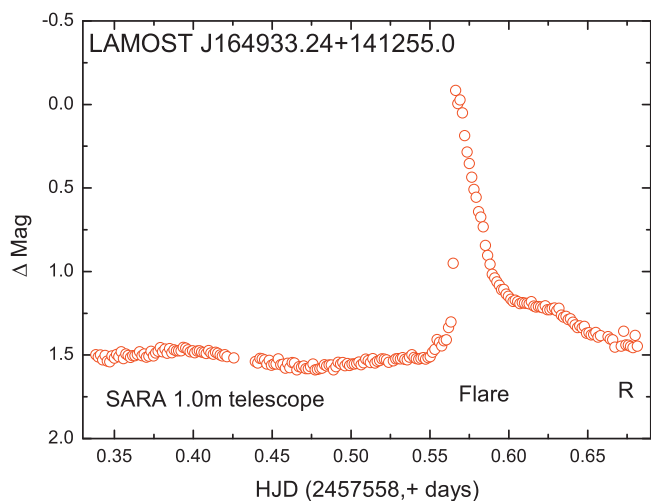

Fig. 12. The first flare event observed on LAMOST J164933.24+141255.0. The flare has a huge amplitude of 1.5 magnitude in the R filter.

References

Abdul-Masih, M., Prša, A., Conroy, K., et al., 2016. Kepler eclipsing binary stars. VIII. Identification of false positive eclipsing binaries and re-extraction of new lightcurves. AJ 151, 101.
Avvakumova, E.A., Malkov, O.Y., Kniazev, A.Y., 2013. Eclipsing variables: Catalogue and classification. AN 334 (8), 860.
Berdyugina, S.V., 2005. Starspots: A key to the stellar dynamo). Living Rev. Solar Phys. 2, 8.
Cui, X.Q., Zhao, Y.H., Chu, Y.Q., et al., 2012. The Large Sky Area Multi-Object Fiber Spectroscopic Telescope (LAMOST). RAA 12, 1197.
De Cat, P., Fu, J.N., Ren, A.B., et al., 2015. Lamost observations in the kepler field. I. Database of low-resolution spectra. ApJS 220, 19.
Dimitrov, D.P., Kjurkchieva, D.P., 2010. GSC2314-0530: the shortest-period eclipsing system with dMe components. MNRAS 406, 2559.
Doyle, J.G., Butler, C.J., van den Oord, G.H.J., et al., 1990. A periodicity in the flaring rate on the eclipsing binary YY Geminorum. A&A 232, 83.
Drake, A.J., Catelan, M., Djorgovski, S.G., et al., 2013a. Probing the Outer Galactic Halo with RR Lyrae from the Catalina Surveys. ApJ 763, 32D.
Drake, A.J., Catelan, M., Djorgovski, S.G., et al., 2013b. Evidence for a milky way tidal stream reaching beyond 100 kpc. ApJ 765, 154.
Drake, A.J., Djorgovske, S.G., Garcia-Alvarez, D., et al., 2014b. Ultra-short period binaries from the Catalina surveys. ApJ 790, 157.
Drake, A.J., Graham, M.J., Djorgovski, S.G., et al., 2014a. The Catalina surveys periodic variable star catalog. ApJS 213, 9.
Eker, Z., Ak, N.F., Bilir, S., et al., 2008. A catalogue of chromospherically active binary stars (third edition). MNRAS 389, 1722.
Fang, X.S., Zhao, G., Zhao, J.K., et al., 2016. Stellar activity with LAMOST - I. Spot configuration in Pleiades. MNRAS 463, 2494.
Frasca, A., Molenda-Zakowicz, J., De Cat, P., Cantanzaro, G., et al., 2016. Activity indicators and stellar parameters of the Kepler targets. An application of the ROTFIT pipeline to LAMOST-Kepler stellar spectra. A&A 594, 39.
Giovannelli, 2008. Cataclysmic variables: A review. Chin J. Astron. Astrophys. 8, 237.
Güdel, M., 2002. Stellar radio astronomy: Probing stellar atmospheres from Protostars to Giants. ARA&A 40, 217.
Hall, J.C., 2008. Stellar chromospheric activity. Living Rev. Solar Phys. 5, 2.
Hartman, J.D., Bakos, G.A., Noyes, R.W., et al., 2011. A photometric variability survey of field K and M dwarf stars with HATNet. AJ 141, 166.
Hawley, S.L., Covey, K.R., Knapp, G.R., et al., 2002. Characterization of M, L, and T dwarfs in the sloan digital sky survey. AJ 123, 3409.
Hawley, S.L., Pettersen, B.R., 1991. The great flare of 1985 April 12 on AD Leonis. ApJ 378, 725.
Hellier, C., 2001. Cataclysmic Variable Stars: How and Why They Vary. Springer-Praxis Press, London.
Hilton, E.J., West, A.A., Hawley, S.L., et al., 2010. M dwarf flares from time-resolved sloan digital sky survey spectra. AJ 140, 1402.
Hoard, D.W., Szkody, P., 1997. Observations of the SW Sextantis Star BH Lyncis in a High State. ApJ 481, 433.
Jiang, D.K., Han, Z.W., Ge, H.W., et al., 2012. The short-period limit of contact binaries. MNRAS 421, 2769.
Karoff, C., Knudsen, M.F., De Cat, P., Bonanno, A., et al., 2016. Observational evidence for enhanced magnetic activity of superflare stars. NatCo 711058.
Keel, W.C., Oswalt, T., Mack, P., et al., 2017. The remote observatories of the Southeastern Association for Research in Astronomy (SARA). PASP 129, 5002.
Kowalski, A.F., Mathioudakis, M., Hawley, S.L., et al., 2016. M dwarf flare continuum variations on one-second timescales: Calibrating and modeling of ULTRACAM flare color indices. ApJ 820, 95.
Kozhevnikova, A.V., Kozhevnikov, V.P., Zakharova, P.E., et al., 2004. The eclipsing variable CM Dra: Surface activity and orbital elements. Astron. Rep. 48, 751.
Kwee, K.K., van Woerden, H., 1956. A method for computing accurately the epoch of minimum of an eclipsing variable. BAN 12, 327.
Liu, X.W., Zhao, G., Hou, J.L., 2015. Preface: The LAMOST Galactic surveys and early results. RAA 15, 1089.
Lohr, M.E., Norton, A.J., Kolh, U.C., et al., 2013. Period and period change measurements for 143 SuperWASP eclipsing binary candidates near the short-period limit and discovery of a doubly eclipsing quadruple system. A&A 549, A86.
Lu, H.P., Zhang, L.Y., Han, X.M., et al., 2016. Photometric follow up investigations on LAMOST survey target Ly And. NewA 48, 58.
Lucy, L.B., 1967. Gravity-darkening for stars with convective envelopes. Z. Astrophys. 65, 89.
Luo, A.L., Zhang, H.T., Zhao, Y.H., Zhao, G., et al., 2012. Data release of the LAMOST pilot survey. RAA 12, 1243.
Luo, A.L., Zhao, Y.H., Zhao, G., et al., 2015. The first data release (DR1) of the LAMOST regular survey. RAA 15, 1095.
McQuillan, A., Mazeh, T., Aigrain, S., 2014. Rotation periods of 34,030 Kepler main-sequence stars: The full autocorrelation sample. ApJs 211, 24.
Messina, S., Rodonò, M., Guinan, E.F., 2001. The "rotation-activity connection": Its extension to photospheric activity diagnostics. A&A 366, 215.
Montes, D., López-Santiago, J., Gálvez, M.C., et al., 2001. Late-type members of young stellar kinematic groups - I. Single stars. MNRAS 328, 45.
Norton, A.J., Wheatley, P.J., West, R.G., et al., 2007. New periodic variable stars coincident with ROSAT sources discovered using SuperWASP. A&A 467, 785.
Olson, E.C., Etzel, P.B., 2015. RX geminorum: Photometric solutions, (nearly uniform) gainer rotation, donor radial velocity solution, Non-LTE accretion disk models of halpha emission profiles, and secular light curve changes in the 20th century. AJ 149, 125.
Palaversa, L., Ivezic, Z., Eyer, L., et al., 2013. Exploring the variable sky with LINEAR. III. Classification of periodic light curves. AJ 146, 101.
Pi, Q.F., Zhang, L.Y., Li, Z.M., et al., 2014. Magnetic activity and orbital period variation of the short-period eclipsing binary DV Psc. AJ 147, 50.
Pojmanski, G., 1997. The all sky automated survey. AcA 47, 467.
Pojmanski, G., Pilecki, B., Szczygiel, D., 2005. The all sky automated survey. Catalog of

variable stars. V. Declinations 0 arcd - +28 arcd of the Northern Hemisphere. AcA 55, 275.

Pollacco, D., Skillen, I., Cameron, A.C., et al., 2006. The WASP project and the SuperWASP cameras. PASP 118, 1407.

Pribulla, T., Vaňko, M., Ammler-von Eiff, M., et al., 2012. The dwarf project: Eclipsing binaries - precise clocks to discover exoplanets. AN 333, 754.

Prša, A., Batalha, N., Slawson, R.W., et al., 2011. Kepler eclipsing binary stars. I. Catalog and principal characterization of 1879 eclipsing binaries in the first data release. AJ 141, 83.

Qian, S.B., Zhang, J., Zhu, L.Y., et al., 2012. Optical flares and flaring oscillations on the M-type eclipsing binary CU Cancri. MNRAS 423, 3646.

Qu, Z.N., Jian, L.q., Liu, J., et al., 2017. The first photometric investigation of the ne-glected short period binary DY CVn. NewA 54, 103.

Reipurth, B., Pedrosa, A., Lago, M.T.V.T., 1996. H alpha emission in pre-main sequence stars. I. an atlas of line profiles. A&AS 120, 29.

Rucinski, S.M., 1973. The W UMa-type systems as contact binaries. I. Two methods of geometrical elements determination. degree of contact. Acta Astron. 23, 79.

Sesar, B., Stuart, J.S., Ivezic, Z., et al., 2011. Exploring the variable Sky with LINEAR. I. Photometric recalibration with the sloan digital sky survey. AJ 142, 190.

Sobolev, V.M., Vyalshin, G.F., Nagovitsyn, Y.A., 1982. Relative intensities of the H_8 and He 3889 lines in the solar chromosphere according to data of the total solar eclipse on June 30, 1973.

Strassmeier, K.G., 2009. Starspots. A&ARev 17, 251.

Strassmeier, K.G., Hall, D.S., Fekel, F.C., et al., 1993. A catalog of chromospherically active binary stars (second edition). A&AS 100, 173.

Szkody, P., Anderson, S.F., Agueros, M., et al., 2002. Cataclysmic variables from the sloan digital sky survey. I. The first results. AJ 123, 430.

Szkody, P., Anderson, S.F., Brooks, K., et al., 2011. Cataclysmic variables from the sloan digital sky survey. VIII. The final year (2007-2008). AJ 142, 181.

Van Hamme, W., 1993. New limb-darkening coefficients for modeling binary star light curves. AJ 106, 2096.

Vida, K., Oláh, K., Ko v ári, Z., et al., 2009. Photospheric and chromospheric activity in V405 Andromedae. An M dwarf binary with components on the two sides of the full convection limit. A&A 504, 1021.

Wang, S.G., Su, D.Q., Chu, Y.Q., et al., 1996. Special configuration of a very large Schmidt telescope for extensive astronomical spectroscopic observation. Appl. Opt. 35, 5155.

Wei, P., Luo, A.L., Li, Y.B., et al., 2013. Mining unusual and rare stellar spectra from large spectroscopic survey data sets using the outlier-detection method. MNRAS (431), 1800.

West, A.A., Hawley, S.L., Walkowicz, L.M., et al., 2004. Spectroscopic properties of cool stars in the sloan digital sky survey: An analysis of magnetic activity and a search for subdwarfs. AJ 128, 426.

West, A.A., Morgan, D.P., Bochanski, J.J., et al., 2011. The sloan digital sky survey data release 7 spectroscopic M dwarf catalog. I. Data. AJ 141, 97.

Wils, P., Lampens, P., van Cauteren, P., et al., 2010. The highly active low-mass eclipsing binary BS UMa. IBVS 5940, 1.

Wilson, R.E., 1979. Eccentric orbit generalization and simultaneous solution of binary star light and velocity curves. ApJ 234, 1054.

Wilson, R.E., 1990. Accuracy and efficiency in the binary star reflection effect. ApJ 356, 613.

Wozniak, P.R., et al., 2004. Northern sky variability survey: Public data release. AJ 127, 2436.

Wu, Y., Luo, A.L., Li, H.N., et al., 2011. Automatic determination of stellar atmospheric parameters and construction of stellar spectral templates of the Guoshoujing Telescope (LAMOST). RAA 11, 924.

Yao, X., Wang, L., Wang, X., et al., 2015. Photometry of variable stars from the THU-NAOC transient survey. I. The first two years. AJ 150, 107.

Yi, Z.P., Luo, A.L., Song, Y.H., et al., 2014. M dwarf catalog of the LAMOST pilot survey. AJ 147, 33.

Zhang, L.Y., Pi, Q.F., Han, X.M., et al., 2016. Chromospheric activity on late-type star DM UMa using high-resolution spectroscopic observations. NewA 44, 66.

Zhang, L.Y., Pi, Q.F., Yang, Y.G., 2014. Magnetic activity and orbital periods of five low-mass eclipsing binaries. MNRAS 442, 2620.

Zhang, L.Y., Pi, Q.F., Zhu, Z.Z., 2015. Chromospheric activity in several single late-type stars. RAA 15, 252.

Zhang, L.Y., Yue, Q., Lu, H.P., et al., 2017. Radio stars observed in the LAMOST spectral survey. RAA 17, 10.

Zhao, G., Zhao, Y.H., Chu, Y.Q., et al., 2012. LAMOST spectral survey — An overview. RAA 12, 723.